

Cool topoclimates promote cold-adapted plant diversity in temperate mountain forests.

Jeremy Borderieux^{1,2}, Emiel De Lombaerde^{3,4}, Karen De Pauw⁴, Pieter Sanczuk⁴, Pieter Vangansbeke⁴, Thomas Vanneste⁴, Pieter De Frenne⁴, Jean-Claude Gégout¹, Josep M. Serra-Diaz^{1,5}.

1. Université de Lorraine, AgroParisTech, INRAE, UMR Silva, 54000 Nancy, France.
2. Department of Forest and Conservation Sciences, Faculty of Forestry, University of British Columbia, Vancouver, British Columbia, Canada
3. Research Institute for Nature and Forest (INBO), Brussels, Belgium
4. Forest & Nature Lab, Department of Environment, Ghent University, Geraardsbergsesteenweg 267, 9090 Gontrode, Belgium.
5. Botanical Institute of Barcelona (IBB, CSIC - CMCNB), 08038 Barcelona, Spain.

Orcid ID:

Jeremy Borderieux : 0000-0003-3993-1067

Emiel De Lombaerde : 0000-0002-0050-2735

Karen De Pauw : 0000-0001-8369-2679

Pieter Sanczuk : 0000-0003-1107-4905

Pieter Vangansbeke : 0000-0002-6356-2858

Thomas Vanneste : 0000-0001-5296-917X

Pieter De Frenne : 0000-0002-8613-0943

Jean-Claude Gégout : 0000-0002-5760-9920

Josep M. Serra-Diaz: 0000-0003-1988-1154

Corresponding author: Jeremy Borderieux: jeremy.borderieux@ubc.ca

Abstract

26 Climate strongly influences the composition and diversity of forest plant
27 communities. Recent studies have highlighted the role of tree canopies in shaping understory
28 thermal conditions at small spatial scales (i.e. microclimate), especially in lowland forests.
29 In mountain forests, however, the influence of topography in environmental conditions (i.e.,
30 topoclimate) is ought to also influence plants' perceived temperature. Understanding how
31 topography and canopies interactively affect understory temperature is key to identifying
32 stable refugia that could shelter cold-adapted forest specialist plants under climate change.

33 Here we report on growing season understory temperatures using 48 loggers in
34 contrasting topographic features and canopy of a mid-range mountain valley spanning from
35 475 m a.s.l. to 1203 m a.s.l. in the Vosges Mountains (NE France). We disentangle the relative
36 importance and the effects of topography vs. canopy in determining local temperatures. We
37 then evaluate how topography and canopy-induced variation in temperature drive plant
38 community composition and richness in 306 floristic surveys across the studied mountain
39 valley.

40 Our results show that topography outweighed canopy cover in explaining growing
41 season understory temperatures. Regardless of canopy, the daily mean temperature of the
42 growing season in south-facing ridges was 1.5 °C (CI: 0.62 - 2.38°C) warmer than shaded
43 valley bottoms, while dense canopies cooled temperatures by 0.5 °C (CI: 0.02 - 0.98 °C)
44 compared to open canopies. Topoclimate explained community composition as much as
45 elevation and was the only significant predictor of species richness. Cold topoclimate
46 harbored 30% more species than the average species richness across our plots. This increase
47 in species richness was explained by an increase of cold-adapted species, both forest
48 specialist and generalist species.

49 Our findings highlight a stronger role of topography compared to canopy cover on
50 community composition in mountain forests via topoclimatic cooling of north-facing slopes
51 and valley bottoms. The importance of topographic features to explain temperature cooling
52 and diversity underpins their role as present and future microrefugia.

53 **Keywords**

54 Community ecology, forest, topoclimate, microclimate, topography, climatic refugia,
55 diversity, understory vegetation.

56 1. Introduction

57 The study of topography influences on vegetation has fascinated ecologists for more
58 than 150 years (Johnston *et al.*, 1848), and has further gained in relevance in the context of
59 the 21st century climate warming (Ashcroft, 2010; Dobrowski, 2011; IPCC, 2021; Lenoir *et*
60 *al.*, 2017). Species distribution and climatic conditions are often modeled at a coarse
61 resolution (typically 1 km or coarser), and thereby fail to capture local variation of climate
62 at finer grains (Franklin *et al.*, 2013) :for instance, the topoclimate shaped by terrain and
63 the forest-induced microclimate (Bramer *et al.*, 2018; De Frenne *et al.*, 2021; Kemppinen *et*
64 *al.*, 2023). Enhanced predictive power obtained by using smaller grain climatic data confirms
65 that species physiological limits are better captured by topography and forest microclimate
66 (Haesen *et al.*, 2023). Given that these factors can attenuate warm macroclimate
67 temperatures, their study is key to identify areas where local conditions are continually
68 buffered in a warmer future (Ashcroft, 2010; De Frenne *et al.*, 2021; Haesen *et al.*, 2023;
69 Hannah *et al.*, 2014). Such areas, refugia, are of utmost importance as they can host source
70 populations of cold-adapted species endangered by climate change. Protection offered these
71 refugia can be disrupted in when it is induced by tree canopies whereas topography-induced
72 buffering is more stable (Ashcroft, 2010; Hylander *et al.*, 2022). As these buffers coexist in
73 temperate mountainous forests, determining which buffering process is at play will allow to
74 better predict and map sources of biodiversity persistence.

75 Variation in aspect can create contrasting local temperatures as slopes oriented to
76 the equator receive more solar radiation, and west-facing slopes receive radiation during
77 the warmest period of the day. As a result, southwest-facing slopes in northern hemisphere
78 mountains display warmer mean temperatures, longer growing seasons and shorter snow
79 cover durations (Ashcroft *et al.*, 2008; Davis *et al.*, 2019; Rita *et al.*, 2021; Rolland, 2003).
80 The physical properties of air also interact with topographic features such as hydrological
81 basins (McLaughlin *et al.*, 2017), valley bottoms and sinks. This phenomenon creates local
82 areas of cold and dense air pooling that decouple, i.e. remove any correlation, between
83 local conditions from the regional climate (Gudiksen *et al.*, 1992; Pastore *et al.*, 2022), thus
84 creating topographic refugia (Dobrowski, 2011). These temperature variations are observed
85 on a moderate scale, from fifty to hundreds of meters, and will be called hereafter
86 topoclimate (Lenoir *et al.*, 2013). To focus on moderate scale and magnitude variation in
87 temperature, we exclude from our definition of topoclimate the lapse rate induced from
88 elevation, as this process has a much stronger effect on temperature, comparable to
89 macroclimatic variation (Lenoir *et al.*, 2013; Rolland, 2003).

90 The topoclimate interacts with what we define as forest-induced microclimate (with
91 smaller scale variation, from a meter to tenth of meter) to jointly determine the understory
92 temperature experienced by forest organisms (De Frenne *et al.*, 2021). Canopy shading and
93 evapotranspiration lead to an overall decrease of temperature throughout the year,
94 exacerbated in summer by a buffering of high temperatures compared to open-air (De Frenne

95 *et al.*, 2021; Zellweger, Coomes, *et al.*, 2019). These buffering effects are apparent and
96 well documented in temperate lowland forest, but their relative importance in contrast to
97 elevation and topography is less known, and current evidence has not reached consensus
98 (Macek *et al.*, 2019; Vandewiele *et al.*, 2023). In temperate mountain forests, we expect
99 that topography (elevation excluded) displays more variability than canopy cover, placing it
100 as the main driver of understory temperature and thus community composition.

101 Community composition was proven to respond to canopy cover in lowland forests.
102 This is evidenced by the increases of the average thermal optimum of the present species (a
103 proxy of species' affinity to climate) in forests where tree canopy was removed (De Frenne
104 *et al.*, 2013; Dietz *et al.*, 2020; Richard *et al.*, 2021) and where warmer understory
105 temperatures are predicted (Zellweger *et al.*, 2020). This sheltering of cold-adapted species
106 by a dense canopy needs to be compared with the sheltering provided by topography in
107 mountain forests, as topographical refugia are likely to offer longer-term buffering of
108 temperature, whereas canopy cover is prone to sudden perturbation (dieback, windfall, etc.)
109 (Ashcroft, 2010; Finocchiaro *et al.*, 2023). Topographic refugia also harbor cold-adapted
110 flora and host populations of species outside their expected climatic range (Ellis & Eaton,
111 2021; Finocchiaro *et al.*, 2023; Haesen *et al.*, 2023; Macek *et al.*, 2019). In temperate
112 mountain forests, it is possible that the sheltering provided by topography resembles the
113 effect of canopy (e.g. lower maximum temperature, higher humidity). To test this
114 hypothesis, we will also study the species' characteristics, we expect an increase of forest
115 specialists that could demonstrate that topoclimate can mimic understory conditions of
116 dense forests.

117 Here we assessed the effects and relative importance of elevation, topography and
118 canopy cover on *in situ* measured understory temperatures and plant community
119 composition and richness. This partitioning will shed light on whether communities are more
120 responsive to canopy or topographic variability, processes that have very different spatial
121 and temporal patterns. This will allow conservation planning to efficiently target
122 conservation areas. After accounting for the elevation gradient, we specifically asked: (1)
123 Does topography (aspect and topographic position) outweigh canopy in explaining understory
124 temperature? (2) does topography and canopy-induced variation in temperature determine
125 community richness and mean species thermal optimum? (3) Are plant habitat preference
126 and climatic affinity related to understory temperature?

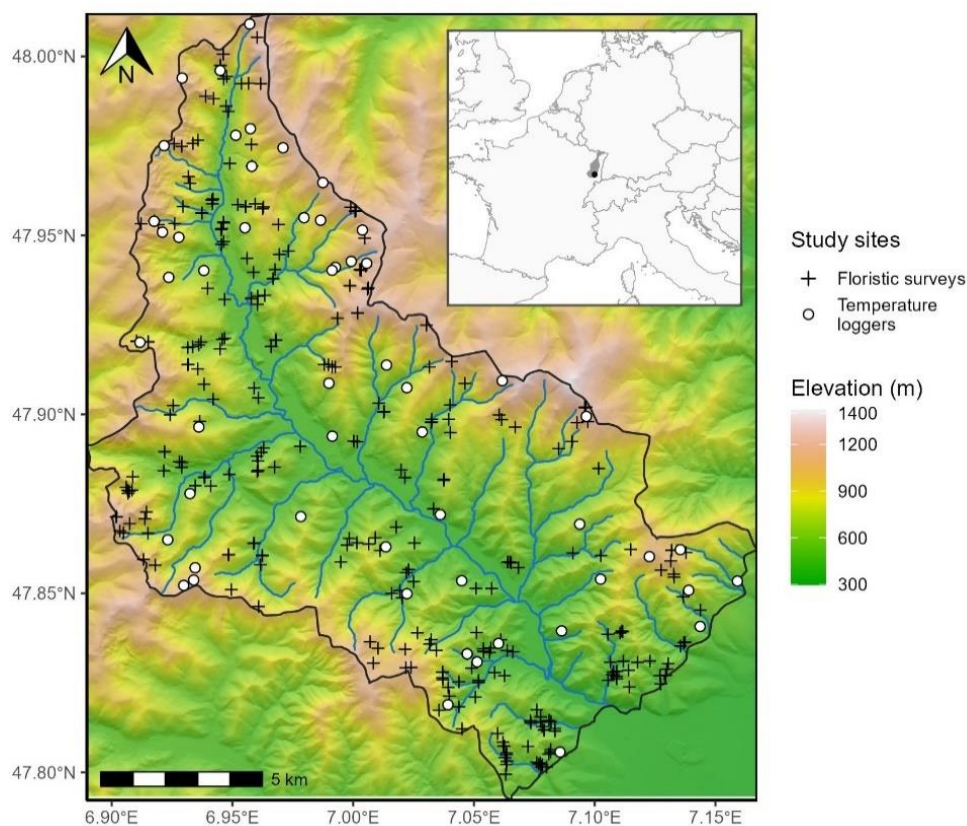
127 **2. Materials and Methods**

128 **2.1. Study Area**

129 Our study region (221 km²) is delineated by the basin of the Thur River, located in
130 one of the southmost valleys of the Vosges Mountain range in France (Figure 1). The Vosges
131 are characterized by a continental climate with harsh winters and short and stormy summers.
132 Its mean annual temperature ranges from 6 °C to 10 °C and precipitation ranges from 800 to

133 2,000 mm year⁻¹(period 1970-2000, Météo France weather stations IGN, 2013). The Thur
 134 River basin is on the warm and dry end gradient of the Vosges Mountains (IGN, 2013).
 135 Forests cover 76% of the Vosges, which transitions from mixed oak stands and monospecific
 136 *Picea abies* stands to mixtures of *Picea abies*, *Abies alba* and *Fagus sylvatica* as elevation
 137 increases (IGN, 2013). The soil of our study region is mostly shallow loam and sand with coarse
 138 elements. The most acidic soils are found at higher altitude because of the dominance of
 139 needles in the humus and the lower temperature at mountaintops (IGN, 2013; Piqué *et al.*,
 140 1994; Thomas *et al.*, 1999). The topography is highly variable, with an elevation ranging
 141 from 400 to 1424 m a.s.l. (but forest occurrence stops past 1250 m a.s.l.) with high
 142 topographic heterogeneity (Figure 1).

143



144
 145 *Figure 1: Study area (black outline) with the location of the temperature loggers (white*
 146 *circles) and the floristic surveys (black crosses). The colored scale represents elevation*
 147 *above sea level, in meters, obtained from a 25-m spatial resolution digital elevation model*
 148 *(IGN, 2017). Hillshade effects have been added to visualize the terrain. The blue line*
 149 *represents the Thur River and its tributaries. The inset shows the Vosges Mountain range*
 150 *(grey) and the location of the studied valley (black point) in western Europe.*

151 2.2. Temperature Predictors

152 We used 25-meter resolution digital elevation model (IGN, 2017) to extract elevation
 153 (m a.s.l.), slope and aspect and to calculate topographical indices. Elevation was kept as is,
 154 as the lapse rate predictor, but does not fall under our definition of topography as we

155 considered it a macroclimatic feature given how much control it has over temperature. Our
156 definition of topoclimatic effect will be focused on smaller scale topographic features
157 described hereafter. We specifically wanted to investigate the difference in radiation
158 received between slopes of differences aspects, a well know driver of topoclimate
159 temperatures, which its effect is less clear under canopy (Macek *et al.*, 2019). We did so by
160 computing the Heat Load Index (HLI). HLI ranges from 0 to 1 (least to most incoming solar
161 radiation) contingent on latitude, slope orientation and steepness, it is a measure of how
162 daily mean temperature is warmed by topographic features most exposed to sunlight, and
163 during the warmest period of the day (south and west slope in the northern hemisphere).

164 To investigate how cold air pooling, dictated by the topography of river basins,
165 influences temperature, we computed a topographic position index (TPI). Cold air pooling
166 ought to be a prominent explanatory factor of community persistence (Finocchiaro *et al.*,
167 2023; Pastore *et al.*, 2022). To do so, we normalized the Euclidian distance between the
168 nearest ridge and nearest thalweg ($TPI = D_{thalweg} / (D_{thalweg} + D_{ridge})$). TPI is the relative
169 position of the cell in the shortest trajectory between a ridge and a drainage basin end,
170 ranging from 0 (valley bottom) to 1 (ridge, Piedallu *et al.*, 2023).

171 We obtained the ‘tree cover density’ from the 2018 product of the Copernicus
172 monitoring service as proxy for local canopy closure (Copernicus, 2018; Sannier *et al.*, 2023).
173 This product consists of a 10-meter resolution percentage of canopy presence within the
174 pixel (ranging from 0 to 100%) and was successfully used before to model microclimate
175 buffering by canopy (Haesen *et al.*, 2021). To validate the assumption that this is a proxy of
176 local canopy closure, and thus microclimatic variation induced by canopy, we correlated it
177 with our field measurements of canopy closure (see below, 2.3 Temperature sampling). We
178 rescaled this product to match the 25-m resolution of our other maps using bilinear
179 interpolation (Hijmans, 2020). We rasterized (25-meter resolution) a 20-meter precision
180 polygon map of French forest (IGN, 2019) to create a mask of the forested area of our study
181 region to limit our analysis and temperature projection to forests, as we only investigate
182 understory flora and temperatures in this study.

183 **2.3. Temperature Sampling**

184 We created a stratified sampling scheme to capture forest understory microclimate
185 variability (Lembrechts *et al.*, 2021; Schweiger *et al.*, 2016). We created 8 elevation strata
186 (spanning 20 m a.s.l. intervals) separated by 102 m. Those strata thus range from [468 - 488]
187 to [1184 - 1204] m a.s.l. They are meant to control for the lapse rate (steady decrease in air
188 temperature as pressure decreases with elevation, Lembrechts *et al.*, 2021), it is the main
189 driver of temperature in the study area but we wanted to separate lapse rate from other
190 topographic features effect.

191 Inside each of these strata, we defined 8 types of plots: 4 plots of below and above
192 the median canopy closure of our study area (90% canopy closure) with a south or a north-
193 facing slope ($HLI > 0.70$ and $HLI < 0.60$, respectively, value chosen to avoid flat terrains of

194 HLI: 0.66). These 4 plots had moderate topographic position indices (between 0.2 and 0.8)
195 and slope ($10^\circ < \text{slope} < 25^\circ$), to avoid confounding their effects with the canopy closure
196 and heat load effects. Additionally, we defined 2 plots with contrasting topographic position
197 indices (lower than 0.2 and higher than 0.8) under high canopy closure and moderate slope.
198 Lastly, we defined 2 plots with contrasting slopes: one on flat ($\text{slope} < 10^\circ$) and one steep
199 ($\text{slope} > 25^\circ$) under high canopy closure and moderate topographic position (summary of the
200 sampling scheme: Table S1). These theoretical strata and plots were designed to systematically
201 cover elevation, HLI, TPI and canopy closure variability, yielding similar results as the PCA-
202 based approach proposed in Lembrechts *et al.*, 2021 as shown in Figure S1.

203 Of the initial 64 theoretical plots spanning the 8 strata, only 59 of the defined
204 situations occurred, mostly because we lacked low topographic position indices (valley
205 bottom) in high elevation classes. We randomly selected one pixel for each plot and stratum
206 located in public forests. We repeated this random drawing 10,000 times and kept the set
207 of plots that maximized the mean minimum distance between plots to reduce spatial
208 autocorrelation.

209 We established the 59 temperature loggers in May 2021 and recorded their location
210 with a GNSS receiver (Trimble TDC600, accuracy= ± 2 m undercover). We placed every logger
211 in public forests to avoid legal constraints (public forest makes up 80% of the forested area
212 in our study region), with no constraints regarding accessibility. We measured canopy closure
213 (0-100%) by a visual observation in a 25-meter radius around the logger. We also estimated
214 canopy closure (0-100%) with a planar picture of the canopy by means of a smartphone
215 (Samsung A40, focal length: 25mm, sensor size: 1/2.8") placed on top of the logger and the
216 sky segmentation 'Glama' application (Tichý, 2016). Plots tagged as low canopy cover were
217 placed accordingly by selecting sites with less than 50% canopy closure as computed by
218 'Glama'. The visual estimation of canopy closure (25-meter radius) was significantly
219 correlated with the remote sensed tree density (R^2 of the linear relationship = 30.0%, Figure
220 S2), but a weak and non-significant correlation was found with the picture analyzed by
221 'Glama' (Figure S2).

222 We recorded air and soil temperatures with TMS-4 loggers (resolution= 0.0625°C ,
223 accuracy= $\pm 0.5^\circ\text{C}$) protected with a radiation shield (Wild *et al.*, 2019). The loggers
224 recorded temperature every 15 minutes until August 2022. We used air temperature 15 cm
225 above the soil surface because it is the most representative temperature experienced by
226 understory plants. We cleaned the time series with the 'myClim' R package (Man *et al.*,
227 2023). More specifically, we removed any duplicates, checked for missing values, and
228 resolved inconsistent time step to the closest 15 minutes default of our loggers. We
229 calibrated the loggers beforehand for a range of -20°C to $+40^\circ\text{C}$ by placing them in a freezer
230 and drying oven along with a T-type thermocouple (accuracy= $\pm 0.2^\circ\text{C}$). From the recorded
231 period, we focused on the growing season (GS hereafter), from 01/04/2023 to 15/08/2023,
232 as it is the most critical period for plant growth. Out of the 59 loggers, 11 were either

233 malfunctioning, stolen, destroyed by animals or displayed erroneous values and were
234 discarded.

235 We checked the capacity of our final sample to cover the variability of our study
236 region following the PCA-based approach of Lembrechts *et al.*, (2021). Our final sampling
237 was able to cover the variability of the valley, except for extreme values of low canopy
238 cover and the unusual valley bottoms of high elevations. The loss of loggers was evenly
239 distributed over plot types, except for the low canopy cover that suffered the most losses
240 (Figure S1).

241 **2.4. Floristic and Species Characteristic Dataset**

242 To test how flora responded to understory temperature, we compiled floristic surveys
243 performed (during the growing season) by students and professors covering soil and climatic
244 transect of the region between 2009 and 2022 (average year= 2015.6). All plots were
245 surveyed for all vascular plant species in the herb layer (smaller than 1 m) and their
246 percentage ground cover was visually estimated. We had 306 floristics surveys in total across
247 the study region. Floristic surveys were performed in 20 x 20 m squares (400 m²) with the
248 GPS position (recorded with built-in tablet GPS; accuracy= \pm 10 m) as the center. We used
249 this position to extract elevation, heat load index, topographic position index and canopy
250 cover for every survey. We harmonized taxonomy to the TaxRef V13 standard (Gargominy,
251 2022). We focused on herbaceous species in the analysis to focus on community dynamics
252 that may reflect shorter-term climate and are less influenced by management than trees or
253 shrubs.

254 One of the objectives of our study is to assess whether local variation of temperature
255 due to topography and canopy benefits cold-adapted species, as they are projected to be
256 the most threatened by climate warming. For this purpose, we used the species' thermal
257 optimum value from ClimPlant V.1.2 (Vangansbeke *et al.*, 2021). These thermal optima are
258 computed from the mean annual temperature ($^{\circ}$ C) within the range of species obtained from
259 Europe-extent distribution atlases and represent the median temperature of the realized
260 niche. Out of the 348 unique recorded species, 309 were assigned a thermal optimum value,
261 covering 90.0% of the occurrences of the whole floristic dataset. We averaged the thermal
262 optimum of every species (without weighting for abundance) of a given survey to obtain the
263 Community Thermal Index (hereafter CTI), which quantifies the thermal preference of the
264 whole community (Borderieux *et al.*, 2023; Vangansbeke *et al.*, 2021). We did not weigh the
265 calculation by species abundance, from a conservation standpoint rarer species may be the
266 most interesting in CTI calculation but may be underrepresented when weighted by
267 abundance. We calculated species richness of a plot as the number of recorded species
268 whether they had an associated thermal optimum in the database or not. By doing so, we
269 wanted to include rare species that were not included in ClimPlant so that our specific
270 richness is representative of the species pool of our study region. The soil of our study region
271 can greatly vary in acidity, we also assigned a pH optimum value obtained from a

272 bioindication database to each species (Gégout *et al.*, 2005), and averaged (not weighted
273 by abundance) it to obtain to control for soil conditions via a bioindicated pH per plot.

274 We used the EuForPlant regional list of forest plant species (Heinken *et al.*, 2022) to
275 assess species habitat affinity. We assigned to each species one of the following affinities:
276 (1.1) species of closed forest (1.2) species which occur in forest edges and openings (2.1)
277 Species which primarily occur in forests but also found in cultural landscapes and forest
278 remnants (2.2) species of open habitats that occurs in forest exclusively through opening
279 and early succession. We excluded species of open vegetation (classified “O”) because of
280 their low number of occurrences (42). In total, 274 species were assigned to an affinity class,
281 covering 85.7% of the occurrences.

282 **2.5. Understory Temperature Modeling**

283 We aggregated the 15-minute frequency time series of the recorded temperature of
284 the growing season 2022 (a warmer than average year, see 3.1) to daily mean and maximum
285 temperature. This aggregation process first removed values outside of the 5th to 95th centile
286 interval of daily values to avoid biasing results due to logger malfunction or a brief burst of
287 sunshine on a logger (thus maximum temperature is the 95th centile). We then averaged the
288 mean or maximum daily temperature to obtain one unique value per logger, the mean daily
289 and maximum daily temperature of the growing season. Having a unique value facilitates
290 the modeling process by removing the need to account for the lack of statistical dependence
291 of temperature time series, and one summary value of the GS is enough as we aim to uncover
292 spatial variation of community composition instead of temporal variation.

293 We wanted to disentangle the relative contribution of lapse rate, topography and
294 canopy to understory temperature, and wanted to map estimates of understory over the
295 study area. To this end, we used a linear model to predict mean and maximum daily
296 temperature of the growing season with elevation, heat load index, topographic position
297 index and remote sensed canopy density as explanatory variables. We preferred remote-
298 sensed canopy cover over the *in-situ* measurements which allowed us to map the
299 temperature models over the entire study area, and thus infer the understory temperature
300 of floristic surveys (mostly without canopy closure records). The warming due to radiation
301 can be tempered when there is canopy to intercept light, canopy buffering is most apparent
302 during the warmest hour of the day (Davis *et al.*, 2019; De Frenne *et al.*, 2021). To account
303 for this, we tested an interaction between heat load index and canopy closure and retained
304 the interaction in the final model if found significant. We checked the assumption of linearity
305 between temperature and its predictors by visually assessing the raw data (Figure S3) and
306 the residuals (Zuur & Ieno, 2016).

307 For each understory temperature model, we did an analytical partitioning of variance
308 to assess which process influenced understory temperature most (Barbosa *et al.*, 2013). The
309 contribution of the predictors was grouped into three groups: elevation, “topoclimate” (TPI
310 and HLI) and “microclimate” (canopy closure). For simplicity and because shared effects had

311 little contribution, we added to each group contribution half of their shared effect to
312 summarize the contribution of the three groups in three numbers.

313 We additionally fitted two linear models with the field measured canopy closure (25
314 m radius observation and planar photography) instead of the remotely sensed measurement
315 to test different methods of canopy closure estimations (Table S2, Table S3).

316 We used the mean understory temperature model ($R^2 = 92.2\%$) to map the
317 contribution of elevation (i.e., lapse rate), of topoclimate (heat load index and topographic
318 position) and of forest-induced microclimate (canopy closure) to the mean understory
319 temperature separately. We mapped the lapse rate by using only the intercept and the
320 elevation parameter. We mapped the topography effect on temperature compared to a
321 reference situation (heat load index of a flat terrain = 0.66 and topographic position index
322 equal to 0.5, prediction of + 1.34°C) and using the two topographic indices. We mapped the
323 contribution of canopy cover by multiplying its parameter to the tree density product, this
324 projection is however extrapolated for the 20% of pixels with a canopy closure lower than
325 79%. This extrapolation was necessary to cover the whole study region and to predict
326 temperature to floristic surveys within those areas. To assess the spatial autocorrelation of
327 the resulting maps (Figure S6), we computed their variogram (scaled semivariance), with a
328 lag of 25 m and a cutoff of 2000 m (Naimi *et al.*, 2014).

329 **2.6. Floristic Composition Analyses**

330 We used a linear model to predict CTI. Species richness being a positive discrete
331 number, we used a negative binomial generalized linear model as overdispersion prevented
332 the use of a Poisson model. The predictors of both models were the contribution to mean
333 understory temperature of elevation, topoclimate and microclimate (the unit of every
334 predictor is thus °C). The soil of our study region can display very different nutrition status
335 and acidity, which can impact both the richness and composition of a community (Degen *et*
336 *al.*, 2005; Koerner *et al.*, 1997; Zellweger *et al.*, 2015). In addition, soil pH is also negatively
337 correlated with elevation (Piqué *et al.*, 1994; Thomas *et al.*, 1999). To account for this,
338 bioindicated pH was also a predictor in the models. We tested that no collinearity between
339 soil acidity and elevation arose when including both by computing a Variance Inflation Factor
340 (VIF, Fox & Weisberg, 2019). For both models, elevation displayed the higher VIF (1.27, well
341 below the threshold of 5, that indicates collinearity, James *et al.*, 2023).

342 We assessed the validity of our models (including temperature models) by testing the
343 assumption of normality and homoscedasticity of the residuals model following (Zuur & Ieno,
344 2016). All assumptions were met (Figure S4). We tested the significant difference from 0 of
345 the estimated parameters with a Wald test.

346 As the 306 surveys uniformly covered the topography effect on temperature (Figure
347 S5), we could split them into three classes of 102 surveys corresponding to a “cold”,
348 “moderate” and “warm” topoclimate effect. The thresholds separating the three classes

349 were determined so that classes have equal number of plots. This discretization allows to
350 directly compare the total occurrence of species, as in Figure 4, thanks to a fixed sampling
351 intensity between classes. It also allows to compute more comprehensive effects of
352 topoclimate over CTI and species richness (e.g. “cold” plots exhibit on average 5 more
353 species than “warm” plots) than with linear estimates. We tested the difference in species
354 richness and CTI between these classes with Wilcoxon rank-sum tests (Rey & Neuhäuser,
355 2011).

356 **2.7. Software**

357 We handled spatial data with the ‘*raster*’ and ‘*sf*’ package (Hijmans, 2020; Pebesma,
358 2018), all the later analyses were carried on with R.4.2.2 (R Core Team, 2019). We computed
359 HLI (McCune & Keon, 2002) using the ‘*spatialEco*’ R package (Evans & Murphy, 2021). We
360 used the ‘*MASS*’ package to fit the negative binomial generalized model (Venables & Ripley,
361 2002). We computed the VIF using the ‘*car*’ package (Fox & Weisberg, 2019). Microclimate
362 temperatures were cleaned using the ‘*myClim*’ R package (Man *et al.*, 2023). We used
363 ‘*ggplot2*’ and ‘*ggspatial*’ packages for data visualization (Dunnington & Thorne, 2020;
364 Wickham, 2011). We performed variance partitioning with the ‘*modEVA*’ package (Barbosa
365 *et al.*, 2013).

366 **3. Results**

367 **3.1. Environmental Determinant of the Understory Microclimate**

368 The growing season (GS) temperature of 2022 was above average (mean GS
369 temperature of the period 2005-2020=11.6 °C, mean 2022 GS temperature=13.2 °C,
370 Markestein weather station (1,184 m a.s.l), (Météo France, 2024)). As a result, the mean
371 daily temperature of the understory (15 cm above the soil surface) was 14.6 °C and spanned
372 between 11.9 °C to 17.5 °C for the higher (1203 m a.s.l) and lower (475 m a.s.l) elevation
373 sensors, respectively. The mean daily maximum temperature of the GS was 19.3 °C and
374 reached a maximum of 24.7 °C for the lowest elevation plots.

375 Elevation was the primary driver of mean temperature variation, with a lapse rate
376 estimated at $-0.68\text{ °C }100\text{m}^{-1}$ (Table 1). The model revealed that HLI - contingent on aspect
377 and slope - was the second driver of mean temperature, which can vary up to 1 °C between
378 low and high radiation slopes. Topographic position also had a significant effect on
379 temperature: the mean temperature was 0.56 °C lower in the bottom of a valley compared
380 to ridges. Lastly, canopy closure (remotely sensed) cooled understory temperatures. An
381 increase of 20% of total canopy cover resulted in a decrease of 0.57 °C. The lapse rate
382 explained 87.4% of the variation in mean temperature, the topographic factors (heat load
383 and topographic position index) 3.95%, and canopy cover accounted for 0.82%. The R^2 of the
384 linear model was 92.2%.

385 The same predictors except for topographic position were significant in the mean
 386 daily maximum temperature model. The heat load index had a higher contribution (21.5%)
 387 in the maximum temperature compared to the mean temperature model, daily maxima
 388 varied for 3.3 °C between low and high heat load indices (Table S4).

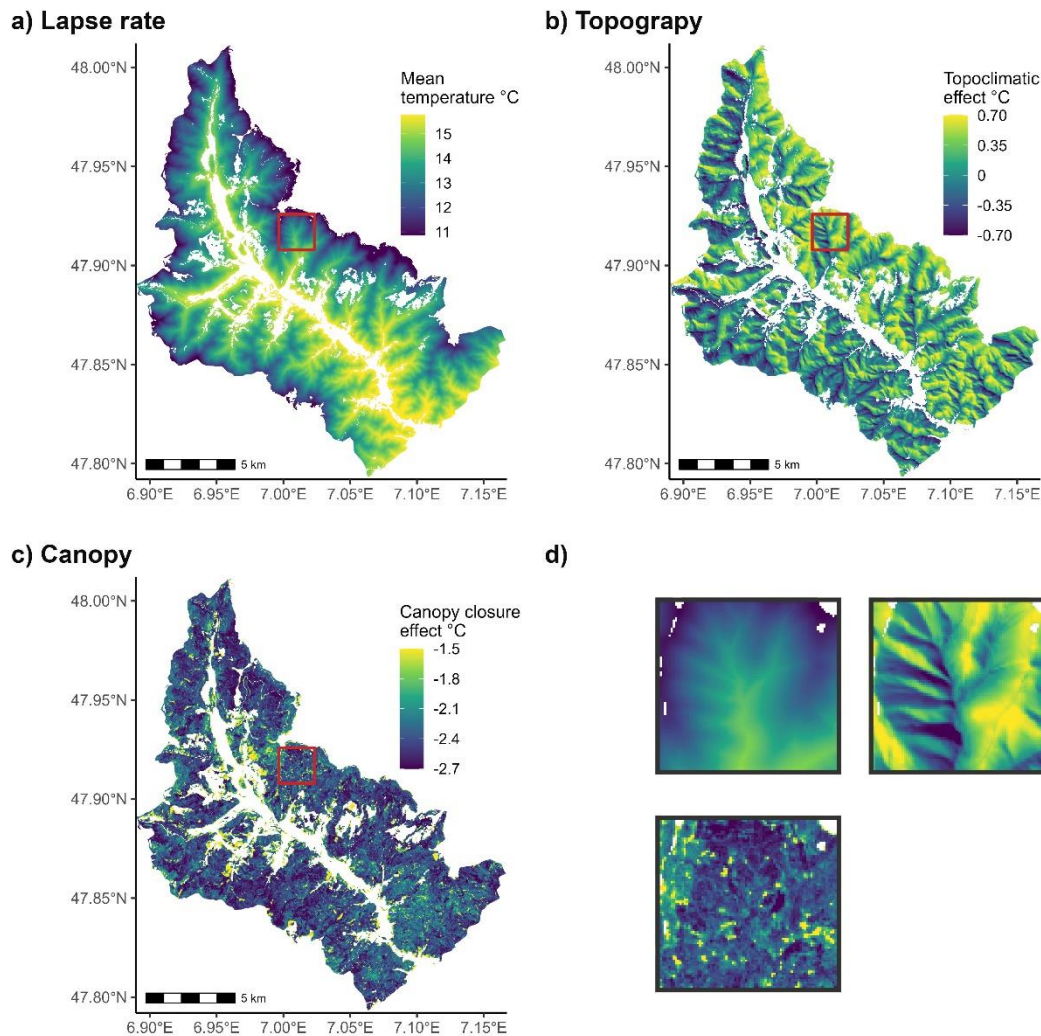
389 Same models where remotely-sensed canopy closure was replaced with field-
 390 measured canopy closure showed overall similar trends, but with difference in estimates
 391 significance. Canopy cover visually estimated in a 25-meter radius was not significant in
 392 predicting mean temperature (Table S2). Immediate canopy cover (smartphone
 393 photography) above the logger explained significantly mean temperature with an interaction
 394 with heat load index, low immediate canopy cover in high radiation slopes displayed warmer
 395 mean temperature (Table S3).

396 *Table 1: Estimated parameters, their standard error and p-values of the predictors included*
 397 *in models of the daily mean growing season temperature. The range of the predictors in*
 398 *the calibration dataset and their standardized effect size on the temperature (standard*
 399 *deviation * estimate) are displayed. The percentage of explained variation per type of*
 400 *predictor is included. P-values were obtained with a Wald test on parameters. Heat load*
 401 *and topographic position have no units (n.u), refer to the methods for their calculation.*

Predictor	Type of predictor	Estimate	Standard error	Range	Effect size (°C)	Explained variation (%)	P-value
Intercept (°C)		21,1	1,11				<10 ⁻⁴
Elevation (m a.s.l.)	Elevation	-0.00684	0.000311	475 : 1203	-1.50	87.4	<10 ⁻⁴
Heat load index (n.u)	Topoclimate	1.53	0.333	0.34 : 0.95	0.30	3.95	<10 ⁻⁴
Topographic position (n.u)		0.656	0.276	0.15 : 1	0.16		0.0220
Canopy closure (%)	Microclimate	-0.0272	0.0115	79.0: 100	-0.16	0.817	0.0229

402

403 **Error! Reference source not found.** The spatial variation of elevation, topography
 404 and canopy closure reveals a complex and fine-grained contribution of this factors to the
 405 forest understory climate (Figure 2). We mapped the individual contributions of elevation
 406 (Figure 2.a), topoclimate (heat load index and topographic position summed; Figure 2.b) and
 407 canopy cover (i.e., microclimate; Figure 2.c) in the study area. We observed strong effects
 408 on understory temperatures caused by steep spatial difference of elevation, topography and
 409 fine-grained canopy cover (Figure 2.d). Lapse rate autocorrelation peaked at 6000 m,
 410 topography in was autocorrelated in a moderate scale 750 m, canopy-induced variation in
 411 temperature autocorrelated in the smallest scale and peaked at 450 m (Figure S6). We used
 412 this map and model to predict the mean understory temperature, and the contribution of
 413 the three components described above for further community composition analyses.



415
 416 *Figure 2: a) Elevation induced change in mean growing season understory temperature of*
 417 *the growing season (lapse rate of $-0.68^{\circ}\text{C } 100\text{ m}^{-1}$), assuming a canopy closure of 90% and*
 418 *no effect from topography. b) mean understory temperature effect induced by topography*
 419 *(heat load and topographic position, i.e. topography) assuming an average canopy cover*
 420 *(90%), compared to a moderate situation (flat terrain midslope). c) mean understory*
 421 *temperature cooling induced by canopy closure assuming no effect from topography. For*
 422 *visualization purposes only we restrained the minimal cooling to -1.5°C , however some*
 423 *pixels displayed lower values up to 0°C due to low to no canopy closure. d) 2 km per 2 km*
 424 *zoomed inset of the red square of the other panels, their color gradient corresponds to the*
 425 *color scale presented in the other panels a-c, respectively. Blank pixels represent land*
 426 *covers other than forests or forests outside of the study region. Linear model R^2 : 92.2%.*

427 **3.2. Microclimatic Determinants of the Floristic Composition**

428 Floristic surveys harbored on average 19 herbaceous species (s.d. 10.7), the mean
 429 community thermal index (CTI) was 7.8°C (s.d. 0.55). Bioindicated soil pH contributed
 430 significantly to CTI and species richness (Table 2). More acidic soils had less diverse and cold-

431 adapted communities. Even if soil is a strong explanatory factor, the overall linear CTI model
 432 explained a moderate amount of variability (R^2 : 35.6%).

433 After soil pH, elevation-induced (lapse rate) and topoclimate were the main predictor
 434 of CTI, of comparable importance (effect size of 0.14 and 0.12 respectively). Topographic
 435 effect was also a significant predictor of species richness, of major importance (an increase
 436 of 1.5 species per plot per increase of one standard deviation of topographic effect, Table
 437 2). The lapse rate was not significant in explaining species richness (Table 2). The forest-
 438 induced microclimate was not a significant predictor in any of the models (Table 2). We
 439 focused the subsequent community analysis around topoclimatic effects, as canopy cooling
 440 did not significantly explain the species richness nor CTI.

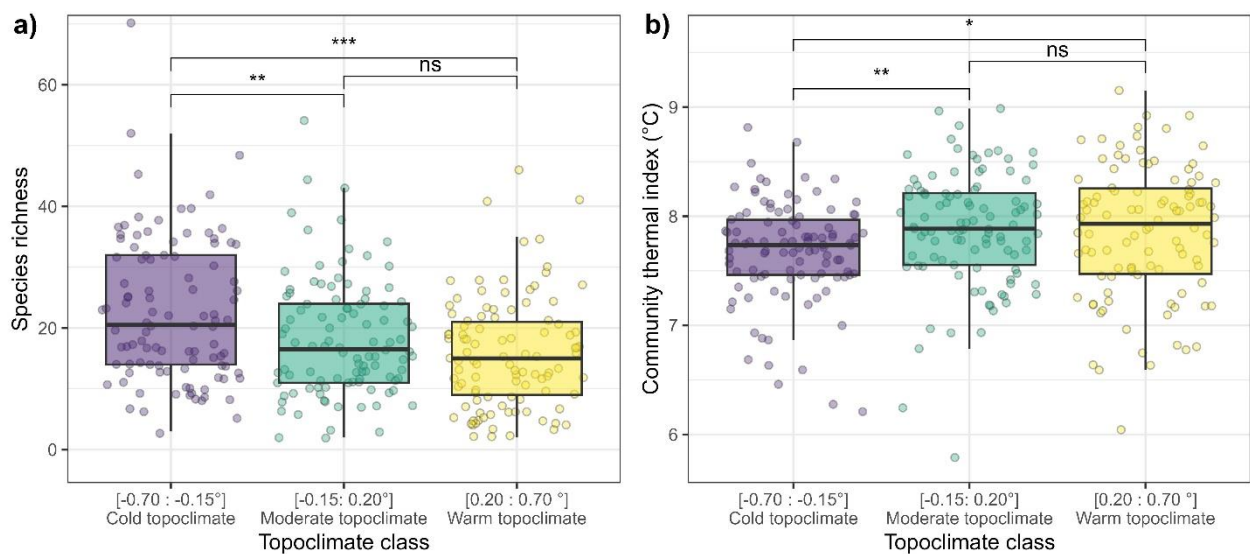
441 Mean and maximum temperature were highly correlated (Pearson coefficient: 0.86),
 442 as a result, a similar effect on flora is found when using predicted effect on max temperature
 443 instead of mean temperature, with a small decrease in fit quality (-1.4% in R^2 for CTI model,
 444 -6 in log-likelihood for the species richness model, Table S5).

445 *Table 2: Estimated parameters, their standard error and p-values of the predictors of the*
 446 *community thermal index (CTI) linear model, and the species richness negative binomial*
 447 *generalized linear model. The range of the predictors and their standardized effect size*
 448 *on the community predicted variable (standard deviation * estimate) are displayed. The P-*
 449 *value is obtained by a Wald test on the parameter.*

Model	Predictor	Estimate	Standard error	Range	Effect size	P-value
Species richness	Intercept (°C)	0.212	0.403			0.598
	Lapse rate (°C)	0.0218	0.0187	12.6 : 18.5	0.46	0.243
	Topography effect (°C)	-0.38	0.0795	-1.55 : -0.13	-1.50	<10 ⁻⁴
	Canopy cooling (°C)	0.0439	0.121	-2.72 : -1.31	0.13	0.716
	Bioindicated pH	0.406	0.0315	3 : 7.15	5.2	<10 ⁻⁴
Community Thermal Index (°C)	Intercept (°C)	5.18	0.406			<10 ⁻⁴
	Lapse rate (°C)	0.0885	0.0188	12.6 : 18.5	0.14	<10 ⁻⁴
	Topography effect (°C)	0.364	0.0804	-1.55 : -0.13	0.12	<10 ⁻⁴
	Canopy cooling (°C)	-0.0236	0.123	-2.72 : -1.31	-0.049	0.848
	Bioindicated pH	0.272	0.0308	3 : 7.15	0.25	<10 ⁻⁴

450

451 We divided the 306 floristic surveys into cold, moderate and warm topoclimatic
 452 classes each comprised of 102 surveys based on topography-induced change in temperature.
 453 The cold topoclimatic class displayed 23 species on average, while the two other classes
 454 displayed 18.5 species on average (Figure 3.a). This difference of approximately 5 species
 455 was significantly different (Figure 3.a). The mean CTI of the cold topoclimatic class was 7.7
 456 °C, which is significantly lower by 0.19°C than the CTI of the two other classes (Figure 3.b).
 457 No such differences were found when using microclimatic (canopy) cooling was used to
 458 create the classes (Figure S7). This discretization of the dataset displayed similar patterns
 459 as the those observed using the continuous predictors of the linear model (Table 2, Figure
 460 S5).

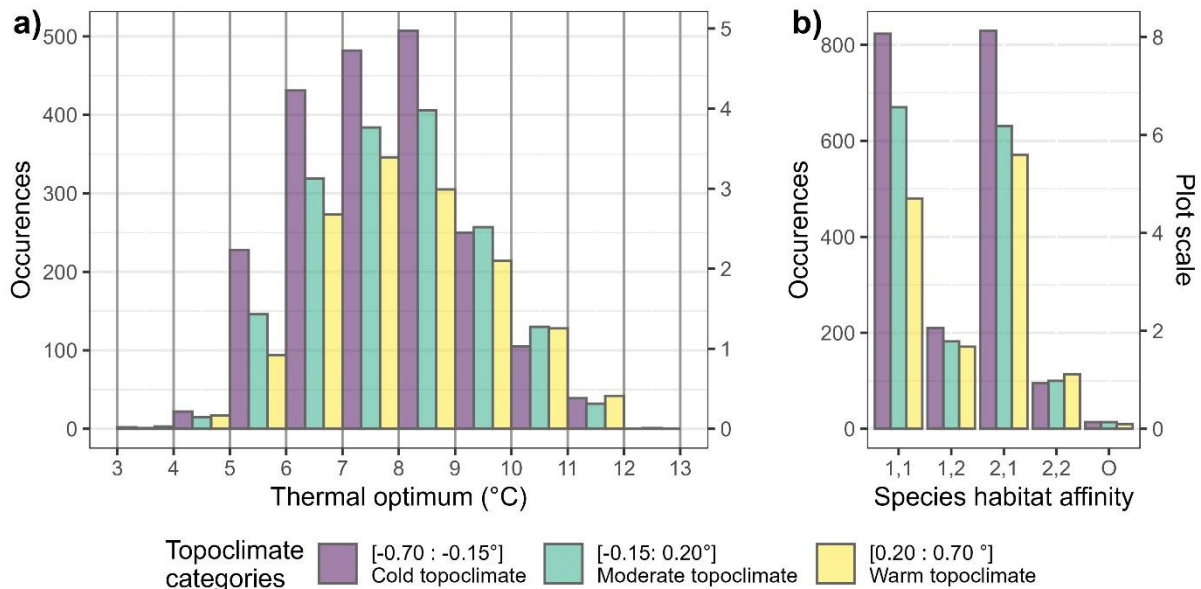


461
 462 **Figure 3: Species richness (a) and community thermal index (b) of 306 floristic surveys**
 463 **evenly spread into three topoclimate classes of even number of plots. The p-value**
 464 **significance of a Wilcoxon test between two classes is displayed as follows: (ns): $p > 0.05$ (*):**
 465 **$p < 0.05$ (**): $p < 0.01$ (***): $P < 0.001$.**

466 The decreases in CTI and the increase in species richness in the cold topoclimatic
 467 class were explained by a surplus of relatively cold-adapted species (i.e. with a species
 468 thermal optimum of 9 °C or less) (Figure 4.a). A two-sided Kolmogorov-Smirnov test
 469 confirmed that the distribution of species thermal optimum in the cold topoclimate class is
 470 significantly different from the other two (P-value against warm = $< 10^{-6}$, P-value against
 471 moderate = 0.00282). No difference in distribution was found between the warm and
 472 moderate class (P-value = 0.18). The plots (n=102 vegetation surveys) in cold topoclimates
 473 displayed in total more than 50 to 100 more occurrences of relatively cold-adapted species
 474 per thermal optimum classes (1°C) than the other two categories (Figure 4.a). The
 475 intermediate topoclimatic class (n=102) also had a higher number of cold-adapted species
 476 compared to the warm topoclimatic class (n=102, Figure 4.a). The cold topoclimatic class
 477 displayed 300 more forest-specialist species occurrences (Heinken *et al.*, 2022) than the
 478 other warmer topoclimatic classes, whereas the occurrences of generalist species increased
 479 by 200 in total (Figure 4.b). We recorded a total of 246, 242 and 223 species (i.e., species

480 pool) in the cold, intermediate and warm topoclimatic classes, respectively. A total of 58,
 481 41, and 33 species were unique to the cold, intermediate and warm topoclimatic classes,
 482 respectively. This means that there are nestedness of species between communities, as
 483 shown in Figure S8.

484



485
 486 *Figure 4: Occurrences of species in the three topoclimatic classes as a function of a) their*
 487 *thermal optimum (°C) and b) their habitat affinity defined by the EuForPlant list as follows:*
 488 *1,1: closed forest mainly 1,2: forest edges and opening 2,1: forest and open vegetation 2,2:*
 489 *mainly in open vegetation (Heinken et al., 2022) The plot-scale occurrence of species is also*
 490 *shown (e.g., 400 occurrences corresponds to approximately 4 species per plots).*

491 4. Discussion

492 We found that both canopy cover and topographic factors strongly influenced
 493 understory temperature during the growing season. We disentangled the elevation gradient
 494 from the topoclimatic and canopy-induced factors by estimating the lapse rate separately,
 495 which was expectably the main driver of understory temperature (Figure 2). After controlling
 496 for the lapse and pH, the temperature cooling by topographic factors (Heat load and
 497 topographic position) was the only significant driver of community composition and richness.
 498 Our understory temperature model allowed us to separately predict the lapse rate,
 499 topoclimatic effect and canopy cover cooling with mean temperature as a unit. This allows
 500 inferring direct links between temperature variation and communities, a necessary step to
 501 advance correlative studies.

502 4.1. Understory temperature determinants

503 The positive correlation found between temperature and heat load can be attributed
 504 to the higher radiation an equator-facing slope receives, which increases both the mean and
 505 daily maximum temperature of the growing season in closed forests. This contrasts with a

506 previous study which only found an effect of heat load on maximum temperature (Macek *et*
507 *al.*, 2019). We measured temperature at 15 cm above the surface, which may explain the
508 higher sensitivity of mean GS temperature to aspect compared to Macek *et al.*, (2019), who
509 measured temperature at 2 m above the surface. Alongside heat load, we found that
510 topographic position influenced mean temperature so that ridges were warmer, and valley
511 bottoms were cooler but had no effect on maximum temperature. We attribute this decrease
512 in temperature to cold air pooling that occurs during nighttime, thus influencing mean daily
513 temperature but with a minimal effect during the hottest hour of the day, when air
514 temperature is homogeneously warm (Smith *et al.*, 2010; Vosper & Brown, 2008). The cooling
515 effect of understory temperature by canopy cover was most apparent for maximum
516 temperature but was also significant for mean temperature, although with a small effect
517 size of -0.16 °C. These observations concur with studies with comparable sampling (Davis *et*
518 *al.*, 2019; Macek *et al.*, 2019).

519 We found that topoclimatic factors outweighed canopy closure in explaining
520 understory temperature in our study area. This finding adds to the current divergent results
521 from Macek *et al.*, (2019) who found no effect of canopy and Vandewiele *et al.*, (2023) who
522 found a predominance of canopy control on temperature in mountain forests. These
523 apparent contrasting results illustrate the complexity and interactions of factors in mountain
524 forest microclimates, potentially depending on site-specific variations in topography and
525 canopy cover, alongside with synoptic conditions leading to difference in transmittance. Our
526 sampling design and subsequent loss of loggers hampered our ability to capture the canopy
527 closure gradient effect on temperature. In our effort of representativeness, our “low
528 canopy” plots displayed a remotely sensed canopy closure of 75%, as there was a dramatic
529 decrease of pixels with values lower than that (Figure S8). However, Zellweger *et al.*, (2019)
530 showed that temperature canopy cooling is more apparent at low canopy cover levels, and
531 saturates past 80% canopy cover. Our limited number of loggers below that threshold could
532 also be the reason why we did not observe a strong effect of canopy on temperature. We
533 argue that our results are interpretable as a comparison of topographic and canopy effects
534 within already forested stands, but not as a comparison of open and closed forests. In
535 previous iterations of the temperature models, we tried to account for the ration of
536 broadleaved and evergreen canopy trees (Díaz-Calafat *et al.*, 2023) but found no significant
537 effect. This could be due to the study period of the growing season, representing leaf-on
538 conditions and thus reducing the difference in canopy buffering induced by lack of leaves in
539 leaf-off conditions.

540 Part of the challenge to determine canopy cover controls in mountain forests stems
541 from the myriads of methods that are used to estimate canopy cover, ranging from
542 hemispheric photographs, terrestrial lidar derived metrics to remotely sensed canopy cover
543 estimations (Ma *et al.*, 2017; Zellweger, De Frenne, *et al.*, 2019). We used Copernicus tree
544 density 2018 satellite images to calibrate the microclimatic model and predict its buffering
545 effect on communities. Remote sensed tree closure density does not account for the vertical

546 profile of trees, which have profound influence on sunlight interception and consequently
547 on understory temperatures (Gril *et al.*, 2023; Zellweger, Coomes, *et al.*, 2019). Remotely
548 sensed canopy cover was significantly but poorly correlated with our field measures (visual
549 estimation and photography). This poor correlation could explain why subsequent prediction
550 of canopy-induced change in temperature failed at explaining community composition and
551 richness. Consistent hemispheric photography of loggers and vegetation plots, or remote
552 sensed lidar offers appealing alternatives to better capture canopy closure variation
553 independent of the topography context.

554 We fitted additional understory temperature models with *in-situ* measurements of
555 canopy cover to conservatively reject canopy cover as prominent driver of microclimate and
556 consequently community composition. These models showed no correlation between
557 understory temperatures and canopy closure except from the interaction between
558 immediate canopy closure (photography) and Heat Load Index (Table S2,

559 Table S3). Previous studies have shown that a localized lack of canopy has stronger
560 warming effect when being located in equator-facing slopes (Davis *et al.*, 2019; Rita *et al.*,
561 2021). This explains why our most local measure of canopy closure only shows a significant
562 interaction. This demonstrates the need to simultaneously study multiple microclimatic
563 drivers and their interactions in mountain ranges (Davis *et al.*, 2019; Greiser *et al.*, 2020).

564 **4.2. Understory temperature effect on communities**

565 We found that temperature variation owing to topography was equally important in
566 shaping a community's affinity to climate compared to that of the elevational gradient
567 (Table 2, after soil pH has been controlled for). This is a consequence of environmental
568 selection pressure on community assembly; Lower temperature at higher altitudes or in
569 topographically shaded slopes can exert a selection pressure on species not adapted to cold
570 whereas lower elevation and high radiation slopes select species not sensitive to late
571 freezing and adapted to warmer temperature (Figure 3, Rita *et al.*, 2021; Wei *et al.*, 2024).
572 Our prediction of both elevation and topography control on mean temperature are quantified
573 the same unit, Celsius degrees °C, but topography-induced temperature effect on
574 community composition is fourfold compared to that of elevation (Table 2). This implies that
575 temperature alone cannot drive the difference in community composition, and other
576 biophysical factors correlated with topography-induced temperature should be at play.
577 Maximum temperature could be a better predictor of the crossing of physiological thresholds
578 dictating species selection (Macek *et al.*, 2019; Pérez-Navarro *et al.*, 2021). However, this
579 hypothesis could not be tested with our dataset as mean and maximum understory
580 temperature were highly correlated. Soil moisture and vapor pressure deficit can also
581 explain the important contribution of topography to communities (Davis *et al.*, 2019).

582 Our topographic position metric relies on hydrography, demonstrating that cold air
583 pooling could occur alongside wetter soils and synergistically favor cold-adapted species not
584 tolerant to drought (Bénichou & Le Breton, 1987; Finocchiaro *et al.*, 2023; Raduła *et al.*,

585 2018). Conversely, ridges and south facing slopes exacerbate the effect of warmer
586 temperature by desiccation, via stronger winds and evaporation, respectively (Davis *et al.*,
587 2019; Piedallu *et al.*, 2023; Rita *et al.*, 2021). These underlying factors altogether can also
588 explain the differences we found in contribution to community composition. They
589 underscore the potential in using several microclimate variables (e.g., mean temperature,
590 vapor pressure deficit) to predict community patterns and species distribution, explicitly
591 considering other microscale biophysical factors in a multivariate fashion (Pérez-Navarro *et*
592 *al.*, 2021). The improvement of mechanistic modeling of microclimate (Maclean, 2020) could
593 also improve predictions of present and future community composition.

594 The cold-adapted communities we observed in cold topoclimates are the result of an
595 increase in relatively cold-adapted species occurrences rather than of a decrease in
596 relatively warm-adapted species (Figure 3). This hints that the constraints on community
597 assembly, in our study region, are a result of temperature becoming too warm for cold-
598 adapted species, rather than otherwise. This increase in occurrences explains the higher
599 specific richness in cold topoclimates (Figure 3). Further to an understory cooling, colder
600 topoclimates could also increase moisture, thus alleviating competition for water during
601 summer and allowing more species to co-occur (Raduła *et al.*, 2018; Sanczuk *et al.*, 2022).
602 Canopy cover has been identified as the driver of the diversity of many taxa in lowland
603 forests due to its buffering of microclimate and light interception (Tinya *et al.*, 2021;
604 Zellweger *et al.*, 2015). Its lower contribution to microclimate variation in mountain forests
605 and the limitation in its measurement mentioned earlier may explain why we do not detect
606 this pattern.

607 Aside from the technical limitations in estimating canopy control on temperature we
608 discussed above, other factors may be at play in explaining the lack of flora response to
609 canopy-induced microclimate. It was outside of the scope of our analysis but explicitly
610 unveiling seasonal microclimatic differences from leaf out timing can help uncover fine
611 community differences such as presence of species vulnerable to cold winter, late freezing
612 and spring ephemeral species. We also showed that after the lapse rate and topoclimate,
613 canopy-induced microclimate is the most variable in space (i.e., spatially autocorrelated in
614 smaller scale, Figure S6). A recent study has shown that plant's thermal preference
615 computed with macroclimate are not responsive to microscale variation in temperature, but
616 rather reflect macroclimatic provenance differences (Gril *et al.*, 2024). Surprisingly,
617 topography, a moderate spatial scale contributor of temperature, had an important effect
618 on these macroscales estimate of plant thermal preference. This demonstrates that
619 topoclimate, being more stable in space and time, can promote cold-adapted species
620 comparably to a macroclimate gradient.

621 **4.3. Implications**

622 How local cooler and wetter conditions are decoupled from the climate warming
623 trend is of utmost importance as they allow for the persistence of cold-adapted species

624 (Greiser *et al.*, 2020; Lenoir *et al.*, 2017), or provide opportunities to facilitate colonization
625 and facilitates range shifts (Serra-Diaz *et al.*, 2015). The thermal heterogeneity topoclimate
626 produced in mountain ranges (Figure 2) should also be considered as a driver of landscape-
627 scale diversity (Stein *et al.*, 2014) and a potential source of community adaptation because
628 species of diverging climatic adaptation coexist in a relatively small area (Hylander *et al.*,
629 2022; Lenoir *et al.*, 2013, 2013). More specifically, our results support the “identifying and
630 protecting microrefugia” section highlighted by Hylander *et al.*, (2022), as north-facing
631 slopes and topographic depressions are easily identifiable from maps, and their cooling
632 capacities and cold-adapted communities can be confirmed by visits in the field.

633 The predominance of topoclimate as a driving force of community composition and
634 richness allows for potential stable refugia to occur. Indeed, buffering of community by
635 canopy alone is prone to disturbances and increased mortality of trees triggered by climate
636 change. Still, a continuity of tree cover in cold topoclimate is recommended, as it ultimately
637 creates the understory microclimate that benefits from such topographic effects. This could
638 be achieved through selective logging and continuous cover silviculture and the reduction of
639 edge effects thanks to buffer zones around the microrefugia. Topography displaying higher
640 control over communities shows that targeting cold topoclimates is an efficient conservation
641 strategy than increasing canopy density in already closed forests. Conservation targeting
642 cold topoclimates is more robust because of the increase in redundancy and biodiversity
643 those locations provide (Figure S8). Additionally, maintaining a connected forest will foster
644 the benefits of the thermal heterogeneity created by topography (Hylander *et al.*, 2022).
645 Indeed, warm topoclimates ought to serve as source populations of species adapted to the
646 current climate, and cold topoclimates have the potential to maintain cold-adapted
647 populations (given sufficient buffering from climate), resulting in a landscape with
648 heterogenous communities.

649 In summary, we show that elevation, topography, and to a lesser extent, canopy
650 closure determines growing season understory temperature in the Vosges mountains in
651 France. Besides elevation, the contribution of topoclimate was the main predictor of
652 community composition and diversity. Understory plant communities of cold topoclimates
653 (north facing slopes and valley bottoms) harbored a higher number of generalist and forest
654 specialist cold-adapted species. Our results place topography as a prominent driver of forest
655 temperature and a key factor to consider for protecting forest cold-adapted species in the
656 context of accelerated global warming.

657 **5. Acknowledgment**

658 The authors are grateful to the Grand Ventron naturel reserve and its director Laurent
659 Domergue for the permission to access the core of the protected forest. The authors
660 acknowledge the National Office for Forests (ONF) for permission to place loggers in public
661 forests. The authors thank the AgroParisTech students and professors involved in the

662 collection of floristic data. The authors thank the funding from a PHC Tournesol mobility
663 grant N° 47550SB. JB Acknowledge the funding from a joint funding from Region Grand Est
664 and AgroParisTech (19_GE8_01020p05035), and was also supported by a . JMSD was funded
665 by the ANR-JCJC (Agence Nationale de la Recherche, jeunes chercheuses et jeunes
666 chercheurs) SEEDFOR (ANR-21-CE32-0003). JMSD acknowledges the support from NASA for
667 UConn's Ecological Modelling Institute (#80NSSC 22K0883) and the program RYC2022-035668-
668 I, funded by MCIU/AEI/10.13039/501100011033 and FSE+.

669 The authors of this preprint declare that they have no financial conflict of interest
670 with the content of this article.

671 6. Data availability

672 The spatial, microclimatic, and floristic data used for this analysis can be found in
673 the repository: https://github.com/Jeremy-borderieux/Article_microclim_vosges.git, and
674 in the archive: <https://zenodo.org/records/12626861> along with the R script that can be
675 used to reproduce the analyses and the figures.

676 7. References

- 677 Ashcroft, M. B. (2010). Identifying refugia from climate change : Identifying refugia from
678 climate change. *Journal of Biogeography*. [https://doi.org/10.1111/j.1365-
679 2699.2010.02300.x](https://doi.org/10.1111/j.1365-2699.2010.02300.x)
- 680 Ashcroft, M., Chisholm, L., & French, K. (2008). The effect of exposure on landscape scale
681 soil surface temperatures and species distribution models. *Faculty of Science - Papers
682 (Archive)*, 211-225. <https://doi.org/10.1007/s10980-007-9181-8>
- 683 Barbosa, A. M., Real, R., Munoz, A. R., & Brown, J. A. (2013). New measures for assessing
684 model equilibrium and prediction mismatch in species distribution models. *Diversity
685 and Distributions*, 19(10), 1333-1338. <https://doi.org/10.1111/ddi.12100>
- 686 Bénichou, P., & Le Breton, O. (1987). Prise en compte de la topographie pour la cartographie
687 de champs pluviométriques statistiques : La méthode Aurelhy. *Colloques de l'INRA*,
688 39(51-69).
- 689 Borderieux, J., Gégout, J.-C., & Serra-Diaz, J. M. (2023). High landscape-scale forest cover
690 favours cold-adapted plant communities in agriculture-forest mosaics. *Global Ecology
691 and Biogeography*, 32(6), 893-903. <https://doi.org/10.1111/geb.13676>
- 692 Bramer, I., Anderson, B. J., Bennie, J., Bladon, A. J., De Frenne, P., Hemming, D., Hill, R.
693 A., Kearney, M. R., Körner, C., Korstjens, A. H., Lenoir, J., Maclean, I. M. D., Marsh,
694 C. D., Morecroft, M. D., Ohlemüller, R., Slater, H. D., Suggitt, A. J., Zellweger, F.,
695 & Gillingham, P. K. (2018). Chapter Three—Advances in Monitoring and Modelling
696 Climate at Ecologically Relevant Scales. In D. A. Bohan, A. J. Dumbrell, G. Woodward,
697 & M. Jackson (Éds.), *Advances in Ecological Research* (Vol. 58, p. 101-161). Academic
698 Press. <https://doi.org/10.1016/bs.aecr.2017.12.005>
- 699 Copernicus. (2018). *High Resolution Layer Tree Cover Density* [Data set].
700 <https://land.copernicus.eu/en/products/high-resolution-layer-tree-cover-density>
- 701 Davis, F. W., Synes, N. W., Fricker, G. A., McCullough, I. M., Serra-Diaz, J. M., Franklin, J.,
702 & Flint, A. L. (2019). LiDAR-derived topography and forest structure predict fine-
703 scale variation in daily surface temperatures in oak savanna and conifer forest

704 landscapes. *Agricultural and Forest Meteorology*, 269-270, 192-202.
705 <https://doi.org/10.1016/j.agrformet.2019.02.015>

706 De Frenne, P., Lenoir, J., Luoto, M., Scheffers, B. R., Zellweger, F., Aalto, J., Ashcroft, M.
707 B., Christiansen, D. M., Decocq, G., De Pauw, K., Govaert, S., Greiser, C., Gril, E.,
708 Hampe, A., Jucker, T., Klinges, D. H., Koelemeijer, I. A., Lembrechts, J. J., Marrec,
709 R., ... Hylander, K. (2021). Forest microclimates and climate change : Importance,
710 drivers and future research agenda. *Global Change Biology*.
711 <https://doi.org/10.1111/gcb.15569>

712 De Frenne, P., Rodriguez-Sanchez, F., Coomes, D. A., Baeten, L., Verstraeten, G., Vellend,
713 M., Bernhardt-Romermann, M., Brown, C. D., Brunet, J., Cornelis, J., Decocq, G. M.,
714 Dierschke, H., Eriksson, O., Gilliam, F. S., Hedl, R., Heinken, T., Hermy, M., Hommel,
715 P., Jenkins, M. A., ... Verheyen, K. (2013). Microclimate moderates plant responses
716 to macroclimate warming. *Proceedings of the National Academy of Sciences*, 110(46),
717 18561-18565. <https://doi.org/10.1073/pnas.1311190110>

718 Degen, T., Devillez, F., & Jacquemart, A.-L. (2005). Gaps promote plant diversity in beech
719 forests (Luzulo-Fagetum), North Vosges, France. *Annals of Forest Science*, 62(5),
720 429-440. <https://doi.org/10.1051/forest:2005039>

721 Díaz-Calafat, J., Uria-Diez, J., Brunet, J., De Frenne, P., Vangansbeke, P., Felton, A.,
722 Öckinger, E., Cousins, S. A. O., Bauhus, J., Ponette, Q., & Hedwall, P.-O. (2023).
723 From broadleaves to conifers: The effect of tree composition and density on
724 understory microclimate across latitudes. *Agricultural and Forest Meteorology*, 341,
725 109684. <https://doi.org/10.1016/j.agrformet.2023.109684>

726 Dietz, L., Collet, C., Dupouey, J.-L., Lacombe, E., Laurent, L., & Gégout, J.-C. (2020).
727 Windstorm-induced canopy openings accelerate temperate forest adaptation to
728 global warming. *Global Ecology and Biogeography*.
729 <https://doi.org/10.1111/geb.13177>

730 Dobrowski, S. Z. (2011). A climatic basis for microrefugia: The influence of terrain on
731 climate. *Global Change Biology*, 17(2), 1022-1035. <https://doi.org/10.1111/j.1365-2486.2010.02263.x>

733 Dunnington, D., & Thorne, B. (2020). ggspatial: Spatial Data Framework for ggplot2. *R*
734 *package version1*, 1.

735 Ellis, C. J., & Eaton, S. (2021). Climate change refugia: Landscape, stand and tree-scale
736 microclimates in epiphyte community composition. *The Lichenologist*, 53(1),
737 135-148. <https://doi.org/10.1017/S0024282920000523>

738 Evans, J. S., & Murphy, M. A. (2021). *spatialEco*.
739 <https://github.com/jeffrejevans/spatialEco>

740 Finocchiaro, M., Médail, F., Saatkamp, A., Diadema, K., Pavon, D., & Meineri, E. (2023).
741 Bridging the gap between microclimate and microrefugia: A bottom-up approach
742 reveals strong climatic and biological offsets. *Global Change Biology*, 29(4),
743 1024-1036. <https://doi.org/10.1111/gcb.16526>

744 Fox, J., & Weisberg, S. (2019). *An R Companion to Applied Regression* (Third). Sage.
745 <https://www.john-fox.ca/Companion/>

746 Franklin, J., Davis, F. W., Ikegami, M., Syphard, A. D., Flint, L. E., Flint, A. L., & Hannah,
747 L. (2013). Modeling plant species distributions under future climates : How fine scale
748 do climate projections need to be? *Global Change Biology*, 19(2), 473-483.
749 <https://doi.org/10.1111/gcb.12051>

750 Franklin, J., Serra-Diaz, J. M., Syphard, A. D., & Regan, H. M. (2016). Global change and
751 terrestrial plant community dynamics. *Proceedings of the National Academy of*
752 *Sciences*, 113(14), 3725-3734. <https://doi.org/10.1073/pnas.1519911113>

753 Gargominy, O. (2022). *TAXREF v13.0, référentiel taxonomique pour la France*. [Data set].
754 UMS PatriNat (OFB-CNRS-MNHN), Paris. <https://doi.org/10.15468/VQUEAM>

- 755 Gégout, J.-C., Coudun, C., Bailly, G., & Jabiol, B. (2005). EcoPlant : A forest site database
756 linking floristic data with soil and climate variables. *Journal of Vegetation Science*,
757 16(2), 257-260. <https://doi.org/10.1111/j.1654-1103.2005.tb02363.x>
- 758 Greiser, C., Ehrlén, J., Meineri, E., & Hylander, K. (2020). Hiding from the climate :
759 Characterizing microrefugia for boreal forest understory species. *Global Change*
760 *Biology*, 26(2), 471-483. <https://doi.org/10.1111/gcb.14874>
- 761 Gril, E., Laslier, M., Gallet-Moron, E., Durrieu, S., Spicher, F., Le Roux, V., Brasseur, B.,
762 Haesen, S., Van Meerbeek, K., Decocq, G., Marrec, R., & Lenoir, J. (2023). Using
763 airborne LiDAR to map forest microclimate temperature buffering or amplification.
764 *Remote Sensing of Environment*, 298, 113820.
765 <https://doi.org/10.1016/j.rse.2023.113820>
- 766 Gril, E., Spicher, F., Vanderpoorten, A., Vital, G., Brasseur, B., Gallet-Moron, E., Le Roux,
767 V., Decocq, G., Lenoir, J., & Marrec, R. (2024). Ecological indicator values of
768 understory plants perform poorly to infer forest microclimate temperature. *Journal*
769 *of Vegetation Science*, 35(2), e13241. <https://doi.org/10.1111/jvs.13241>
- 770 Gudiksen, P. H., Leone, J. M., King, C. W., Ruffieux, D., & Neff, W. D. (1992). Measurements
771 and Modeling of the Effects of Ambient Meteorology on Nocturnal Drainage Flows.
772 *Journal of Applied Meteorology and Climatology*, 31(9), 1023-1032.
773 [https://doi.org/10.1175/1520-0450\(1992\)031<1023:MAMOTE>2.0.CO;2](https://doi.org/10.1175/1520-0450(1992)031<1023:MAMOTE>2.0.CO;2)
- 774 Haesen, S., Lembrechts, J. J., De Frenne, P., Lenoir, J., Aalto, J., Ashcroft, M. B., Kopecký,
775 M., Luoto, M., Maclean, I., Nijs, I., Niittynen, P., van den Hoogen, J., Arriga, N.,
776 Bruna, J., Buchmann, N., Čiliak, M., Collalti, A., De Lombaerde, E., Descombes, P.,
777 ... Van Meerbeek, K. (2021). ForestTemp - Sub-canopy microclimate temperatures of
778 European forests. *Global Change Biology*, 27(23), 6307-6319.
779 <https://doi.org/10.1111/gcb.15892>
- 780 Haesen, S., Lenoir, J., Gril, E., De Frenne, P., Lembrechts, J. J., Kopecký, M., Macek, M.,
781 Man, M., Wild, J., & Van Meerbeek, K. (2023). Microclimate reveals the true thermal
782 niche of forest plant species. *Ecology Letters*, 26(12).
783 <https://doi.org/10.1111/ele.14312>
- 784 Hannah, L., Flint, L., Syphard, A. D., Moritz, M. A., Buckley, L. B., & McCullough, I. M.
785 (2014). Fine-grain modeling of species' response to climate change : Holdouts,
786 stepping-stones, and microrefugia. *Trends in Ecology & Evolution*, 29(7), 390-397.
787 <https://doi.org/10.1016/j.tree.2014.04.006>
- 788 Heinken, T., Diekmann, M., Liira, J., Orczewska, A., Schmidt, M., Brunet, J., Chytrý, M.,
789 Chabrierie, O., Decocq, G., De Frenne, P., Dřevojan, P., Dzwonko, Z., Ewald, J.,
790 Feilberg, J., Graae, B. J., Grytnes, J.-A., Hermy, M., Kriebitzsch, W.-U., Laiviņš, M.,
791 ... Vanneste, T. (2022). The European Forest Plant Species List (EuForPlant) : Concept
792 and applications. *Journal of Vegetation Science*, 33(3), e13132.
793 <https://doi.org/10.1111/jvs.13132>
- 794 Hijmans, R. J. (2020). *raster : Geographic Data Analysis and Modeling*. [https://CRAN.R-](https://CRAN.R-project.org/package=raster)
795 [project.org/package=raster](https://CRAN.R-project.org/package=raster)
- 796 Hylander, K., Greiser, C., Christiansen, D. M., & Koelemeijer, I. A. (2022). Climate
797 adaptation of biodiversity conservation in managed forest landscapes. *Conservation*
798 *Biology*, 36(3), e13847. <https://doi.org/10.1111/cobi.13847>
- 799 IGN. (2013). *Fiches descriptives des grandes régions écologiques (GRECO) et des*
800 *sylvoécorégions (SER)*. <https://inventaire-forestier.ign.fr/spip.php?article773>
- 801 IGN. (2017). *BD ALTI Le modèle numérique de terrain (MNT) maillé qui décrit le relief du*
802 *territoire français à moyenne échelle [Data set]*.
803 <https://geoservices.ign.fr/documentation/donnees/alti/bdalti>
- 804 IGN. (2019). *BD Forêt version 2*. Institut National de l'Information Géographique et
805 Forestière. <https://inventaire-forestier.ign.fr/spip.php?article646>

- 806 IPCC. (2021). Summary for Policymakers. In V. Masson-Delmotte, P. Zhai, A. Pirani, S. L.
807 Connors, C. Péan, S. Berger, N. Caud, Y. Chen, L. Goldfarb, M. I. Gomis, M. Huang,
808 K. Leitzell, E. Lonnoy, J. B. R. Matthews, T. K. Maycock, T. Waterfield, O. Yelekçi,
809 R. Yu, & B. Zhou (Éds.), *Climate Change 2021: The Physical Science Basis. Contribution of Working Group I to the Sixth Assessment Report of the Intergovernmental Panel on Climate Change* (p. 3–32). Cambridge University Press.
810 <https://doi.org/10.1017/9781009157896.001>
- 813 James, G., Witten, D., Hastie, T., Tibshirani, R., & Taylor, J. (2023). *An Introduction to Statistical Learning: With Applications in Python*. Springer International Publishing.
814 <https://doi.org/10.1007/978-3-031-38747-0>
- 816 Johnston, A. K., Brewster, D., & Berghaus, H. K. W. (1848). *The physical atlas: A series of maps & notes illustrating the geographical distribution of natural phenomena* [Map].
817 William Blackwood & Sons.
- 819 Kempainen, J., Lembrechts, J. J., Van Meerbeek, K., Carnicer, J., Chardon, N. I., Kardol,
820 P., Lenoir, J., Liu, D., Maclean, I., Pergl, J., Saccone, P., Senior, R. A., Shen, T.,
821 Słowińska, S., Vandvik, V., von Oppen, J., Aalto, J., Ayalew, B., Bates, O., ... De
822 Frenne, P. (2023). *Microclimate, an inseparable part of ecology and biogeography*.
823 Zenodo. <https://doi.org/10.5281/zenodo.7973314>
- 824 Koerner, W., Dupouey, J. L., Dambrine, E., & Benoit, M. (1997). Influence of Past Land Use
825 on the Vegetation and Soils of Present Day Forest in the Vosges Mountains, France.
826 *Journal of Ecology*, 85(3), 351-358. <https://doi.org/10.2307/2960507>
- 827 Lembrechts, J. J., Lenoir, J., Scheffers, B., & De Frenne, P. (2021). Designing countrywide
828 and regional microclimate networks. *Global Ecology and Biogeography*.
829 <https://doi.org/10.1111/geb.13290>
- 830 Lenoir, J., Graae, B. J., Aarrestad, P. A., Alsos, I. G., Armbruster, W. S., Austrheim, G.,
831 Bergendorff, C., Birks, H. J. B., Bråthen, K. A., Brunet, J., Bruun, H. H., Dahlberg,
832 C. J., Decocq, G., Diekmann, M., Dynesius, M., Ejrnæs, R., Grytnes, J.-A., Hylander,
833 K., Klanderud, K., ... Svenning, J.-C. (2013). Local temperatures inferred from plant
834 communities suggest strong spatial buffering of climate warming across Northern
835 Europe. *Global Change Biology*, 19(5), 1470-1481.
836 <https://doi.org/10.1111/gcb.12129>
- 837 Lenoir, J., Hattab, T., & Pierre, G. (2017). Climatic microrefugia under anthropogenic
838 climate change: Implications for species redistribution. *Ecography*, 40(2), 253-266.
839 <https://doi.org/10.1111/ecog.02788>
- 840 Ma, Q., Su, Y., & Guo, Q. (2017). Comparison of Canopy Cover Estimations From Airborne
841 LiDAR, Aerial Imagery, and Satellite Imagery. *IEEE Journal of Selected Topics in*
842 *Applied Earth Observations and Remote Sensing*, 10(9), 4225-4236.
843 <https://doi.org/10.1109/JSTARS.2017.2711482>
- 844 Macek, M., Kopecký, M., & Wild, J. (2019). Maximum air temperature controlled by
845 landscape topography affects plant species composition in temperate forests.
846 *Landscape Ecology*, 34(11), 2541-2556. <https://doi.org/10.1007/s10980-019-00903-x>
- 847 Maclean, I. M. D. (2020). Predicting future climate at high spatial and temporal resolution.
848 *Global Change Biology*, 26(2), 1003-1011. <https://doi.org/10.1111/gcb.14876>
- 849 Man, M., Kalčík, V., Macek, M., Brůna, J., Hederová, L., Wild, J., & Kopecký, M. (2023).
850 myClim: Microclimate data handling and standardised analyses in R. *Methods in*
851 *Ecology and Evolution*, 14(9). <https://doi.org/10.1111/2041-210X.14192>
- 852 McCune, B., & Keon, D. (2002). Equations for potential annual direct incident radiation and
853 heat load. *Journal of Vegetation Science*, 13(4), 603-606.
854 <https://doi.org/10.1111/j.1654-1103.2002.tb02087.x>
- 855 McLaughlin, B. C., Ackerly, D. D., Klos, P. Z., Natali, J., Dawson, T. E., & Thompson, S. E.
856 (2017). Hydrologic refugia, plants, and climate change. *Global Change Biology*, 23(8),
857 2941-2961. <https://doi.org/10.1111/gcb.13629>

858 Météo France. (2024). *Meteo.data.gouv.fr*. <https://meteo.data.gouv.fr/datasets>

859 Naimi, B., Hamm, N. a s, Groen, T. A., Skidmore, A. K., & Toxopeus, A. G. (2014). Where is
860 positional uncertainty a problem for species distribution modelling. *Ecography*, *37*,
861 191-203. <https://doi.org/10.1111/j.1600-0587.2013.00205.x>

862 Pastore, M. A., Classen, A. T., D'Amato, A. W., Foster, J. R., & Adair, E. C. (2022). Cold-air
863 pools as microrefugia for ecosystem functions in the face of climate change. *Ecology*,
864 *103*(8), e3717. <https://doi.org/10.1002/ecy.3717>

865 Pebesma, E. (2018). Simple Features for R: Standardized Support for Spatial Vector Data.
866 *The R Journal*, *10*(1), 439-446. <https://doi.org/10.32614/RJ-2018-009>

867 Pérez-Navarro, M. Á., Serra-Diaz, J. M., Svenning, J., Esteve-Selma, M. Á., Hernández-
868 Bastida, J., & Lloret, F. (2021). Extreme drought reduces climatic disequilibrium in
869 dryland plant communities. *Oikos*. <https://doi.org/10.1111/oik.07882>

870 Piedallu, C., Dallery, D., Bresson, C., Legay, M., Gégout, J.-C., & Pierrat, R. (2023). Spatial
871 vulnerability assessment of silver fir and Norway spruce dieback driven by climate
872 warming. *Landscape Ecology*, *38*(2), 341-361. <https://doi.org/10.1007/s10980-022-01570-1>

874 Piqué, A., Pluck, P., Schneider, J.-L., & Whitechurch, H. (1994). The Vosges Massif. In J.
875 Chantraine, J. Rolet, D. S. Santallier, A. Piqué, & J. D. Keppie (Éds.), *Pre-Mesozoic*
876 *Geology in France and Related Areas* (p. 416-425). Springer.
877 https://doi.org/10.1007/978-3-642-84915-2_32

878 R Core Team. (2019). *R: A Language and Environment for Statistical Computing*. R
879 Foundation for Statistical Computing. <https://www.R-project.org/>

880 Raduła, M. W., Szymura, T. H., & Szymura, M. (2018). Topographic wetness index explains
881 soil moisture better than bioindication with Ellenberg's indicator values. *Ecological*
882 *Indicators*, *85*, 172-179. <https://doi.org/10.1016/j.ecolind.2017.10.011>

883 Rey, D., & Neuhäuser, M. (2011). Wilcoxon-Signed-Rank Test. In M. Lovric (Éd.),
884 *International Encyclopedia of Statistical Science* (p. 1658-1659). Springer.
885 https://doi.org/10.1007/978-3-642-04898-2_616

886 Richard, B., Dupouey, J.-L., Corcket, E., Alard, D., Archaux, F., Aubert, M., Boulanger, V.,
887 Gillet, F., Langlois, E., Macé, S., Montpied, P., Beaufils, T., Begeot, C., Behr, P.,
888 Boissier, J.-M., Camaret, S., Chevalier, R., Decocq, G., Dumas, Y., ... Lenoir, J.
889 (2021). The climatic debt is growing in the understorey of temperate forests : Stand
890 characteristics matter. *Global Ecology and Biogeography*, *30*(7).
891 <https://doi.org/10.1111/geb.13312>

892 Rita, A., Bonanomi, G., Allevato, E., Borghetti, M., Cesarano, G., Mogavero, V., Rossi, S.,
893 Saulino, L., Zotti, M., & Saracino, A. (2021). Topography modulates near-ground
894 microclimate in the Mediterranean *Fagus sylvatica* treeline. *Scientific Reports*, *11*(1),
895 8122. <https://doi.org/10.1038/s41598-021-87661-6>

896 Rolland, C. (2003). Spatial and Seasonal Variations of Air Temperature Lapse Rates in Alpine
897 Regions. *Journal of Climate*, *16*(7), 1032-1046. [https://doi.org/10.1175/1520-0442\(2003\)016<1032:SASVOA>2.0.CO;2](https://doi.org/10.1175/1520-0442(2003)016<1032:SASVOA>2.0.CO;2)

899 Sala, O. E., Chapin, F. S., Armesto, J. J., Berlow, E., Bloomfield, J., Dirzo, R., Huber-
900 Sanwald, E., Huenneke, L. F., Jackson, R. B., Kinzig, A., Leemans, R., Lodge, D. M.,
901 Mooney, H. A., Oesterheld, M., Poff, N. L., Sykes, M. T., Walker, B. H., Walker, M.,
902 & Wall, D. H. (2000). Global biodiversity scenarios for the year 2100. *Science (New*
903 *York, N.Y.)*, *287*(5459), 1770-1774. <https://doi.org/10.1126/science.287.5459.1770>

904 Sanczuk, P., De Lombaerde, E., Haesen, S., Van Meerbeek, K., Luoto, M., Van der Veken,
905 B., Van Beek, E., Hermy, M., Verheyen, K., Vangansbeke, P., & De Frenne, P. (2022).
906 Competition mediates understorey species range shifts under climate change.
907 *Journal of Ecology*, *110*(8), 1813-1825. <https://doi.org/10.1111/1365-2745.13907>

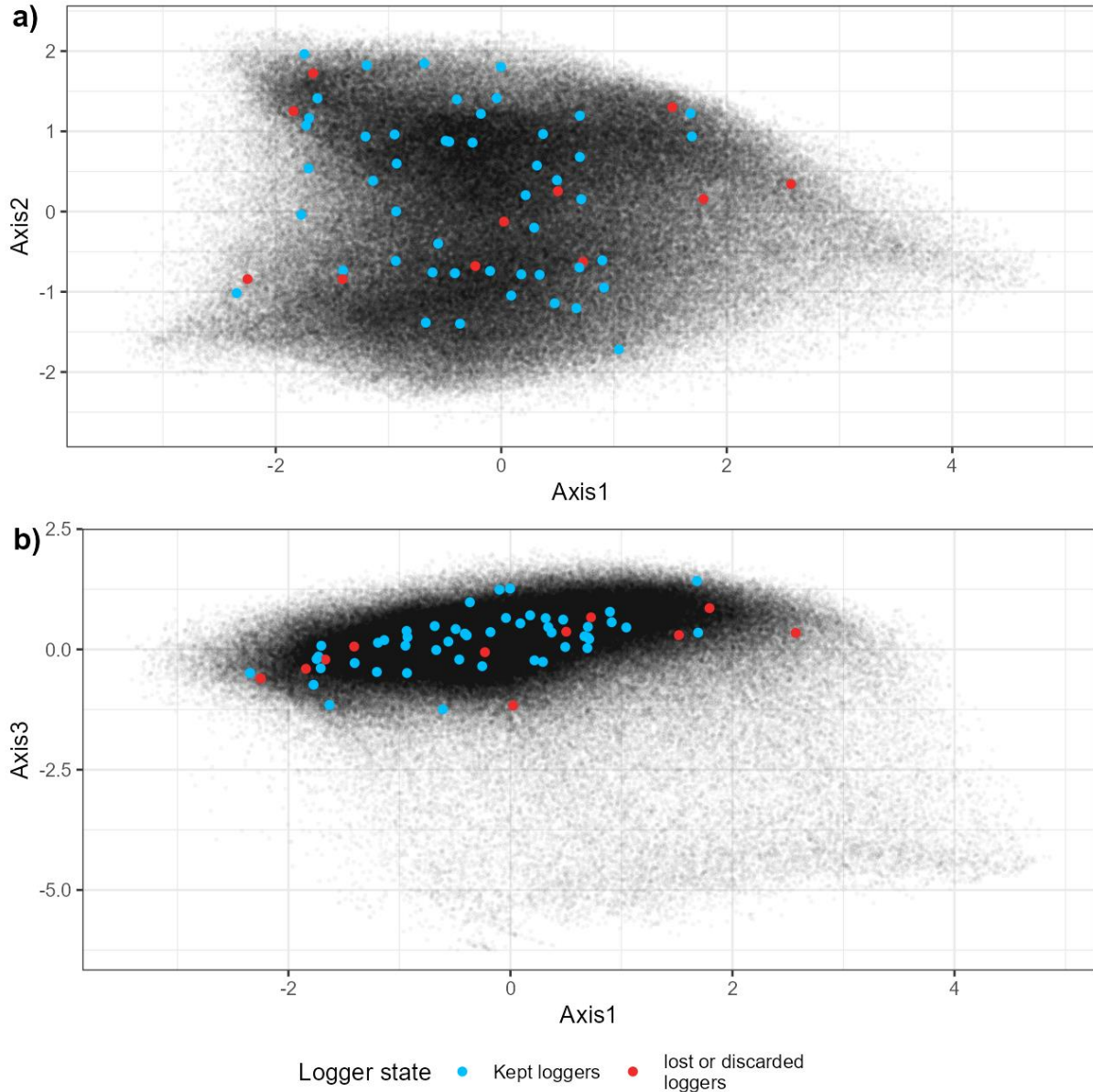
- 908 Sannier, C., Gallego, J., Langanke, T., Donezar, U., & Pennec, A. (2023). Tree cover area
 909 estimation in europe based on the combination of in situ reference data and the
 910 copernicus high resolution layer on tree cover density. *The International Archives of*
 911 *the Photogrammetry, Remote Sensing and Spatial Information Sciences*, XLVIII-M-
 912 1-2023, 277-284. <https://doi.org/10.5194/isprs-archives-XLVIII-M-1-2023-277-2023>
- 913 Schweiger, A. H., Irl, S. D. H., Steinbauer, M. J., Dengler, J., & Beierkuhnlein, C. (2016).
 914 Optimizing sampling approaches along ecological gradients. *Methods in Ecology and*
 915 *Evolution*, 7(4), 463-471. <https://doi.org/10.1111/2041-210X.12495>
- 916 Serra-Diaz, J. M., Scheller, R. M., Syphard, A. D., & Franklin, J. (2015). Disturbance and
 917 climate microrefugia mediate tree range shifts during climate change. *Landscape*
 918 *Ecology*, 30(6), 1039-1053. <https://doi.org/10.1007/s10980-015-0173-9>
- 919 Smith, S. A., Brown, A. R., Vosper, S. B., Murkin, P. A., & Veal, A. T. (2010). Observations
 920 and Simulations of Cold Air Pooling in Valleys. *Boundary-Layer Meteorology*, 134(1),
 921 85-108. <https://doi.org/10.1007/s10546-009-9436-9>
- 922 Stein, A., Gerstner, K., & Kreft, H. (2014). Environmental heterogeneity as a universal driver
 923 of species richness across taxa, biomes and spatial scales. *Ecology Letters*, 17(7),
 924 866-880. <https://doi.org/10.1111/ele.12277>
- 925 Thomas, A. L., Dambrine, E., King, D., Party, J. P., & Probst, A. (1999). A spatial study of
 926 the relationships between streamwater acidity and geology, soils and relief (Vosges,
 927 northeastern France). *Journal of Hydrology*, 217(1), 35-45.
 928 [https://doi.org/10.1016/S0022-1694\(99\)00014-1](https://doi.org/10.1016/S0022-1694(99)00014-1)
- 929 Tichý, L. (2016). Field test of canopy cover estimation by hemispherical photographs taken
 930 with a smartphone. *Journal of Vegetation Science*, 27(2), 427-435.
 931 <https://doi.org/10.1111/jvs.12350>
- 932 Tinya, F., Kovács, B., Bidló, A., Dima, B., Király, I., Kutszegi, G., Lakatos, F., Mag, Z.,
 933 Márialigeti, S., Nascimbene, J., Samu, F., Siller, I., Szél, G., & Ódor, P. (2021).
 934 Environmental drivers of forest biodiversity in temperate mixed forests - A multi-
 935 taxon approach. *Science of The Total Environment*, 795, 148720.
 936 <https://doi.org/10.1016/j.scitotenv.2021.148720>
- 937 Vandewiele, M., Geres, L., Lotz, A., Mandl, L., Richter, T., Seibold, S., Seidl, R., & Senf, C.
 938 (2023). Mapping spatial microclimate patterns in mountain forests from LiDAR.
 939 *Agricultural and Forest Meteorology*, 341, 109662.
 940 <https://doi.org/10.1016/j.agrformet.2023.109662>
- 941 Vangansbeke, P., Máliš, F., Hédl, R., Chudomelová, M., Vild, O., Wulf, M., Jahn, U., Welk,
 942 E., Rodríguez-Sánchez, F., & Frenne, P. D. (2021). ClimPlant: Realized climatic
 943 niches of vascular plants in European forest understoreys. *Global Ecology and*
 944 *Biogeography*, 30(6), 1183-1190. <https://doi.org/10.1111/geb.13303>
- 945 Venables, W. N., & Ripley, B. D. (2002). *Modern Applied Statistics with S* (Fourth). Springer.
 946 <https://www.stats.ox.ac.uk/pub/MASS4/>
- 947 Vosper, S. B., & Brown, A. R. (2008). Numerical Simulations of Sheltering in Valleys: The
 948 Formation of Nighttime Cold-Air Pools. *Boundary-Layer Meteorology*, 127(3),
 949 429-448. <https://doi.org/10.1007/s10546-008-9272-3>
- 950 Wei, L., Sanczuk, P., De Pauw, K., Caron, M. M., Selvi, F., Hedwall, P., Brunet, J., Cousins,
 951 S. A. O., Plue, J., Spicher, F., Gasperini, C., Iacopetti, G., Orczewska, A., Uria-Diez,
 952 J., Lenoir, J., Vangansbeke, P., & De Frenne, P. (2024). Using warming tolerances to
 953 predict understory plant responses to climate change. *Global Change Biology*, 30(1),
 954 e17064. <https://doi.org/10.1111/gcb.17064>
- 955 Wickham, H. (2011). Ggplot2. *WIREs Computational Statistics*, 3(2), 180-185.
 956 <https://doi.org/10.1002/wics.147>
- 957 Wiens, J. J. (2016). Climate-Related Local Extinctions Are Already Widespread among Plant
 958 and Animal Species. *PLOS Biology*, 14(12), e2001104.
 959 <https://doi.org/10.1371/journal.pbio.2001104>

- 960 Wild, J., Kopecký, M., Macek, M., Šanda, M., Jankovec, J., & Haase, T. (2019). Climate at
961 ecologically relevant scales: A new temperature and soil moisture logger for long-
962 term microclimate measurement. *Agricultural and Forest Meteorology*.
963 <https://doi.org/10.1016/j.agrformet.2018.12.018>
- 964 Zellweger, F., Braunisch, V., Morsdorf, F., Baltensweiler, A., Abegg, M., Roth, T., Bugmann,
965 H., & Bollmann, K. (2015). Disentangling the effects of climate, topography, soil and
966 vegetation on stand-scale species richness in temperate forests. *Forest Ecology and*
967 *Management*, 349, 36-44. <https://doi.org/10.1016/j.foreco.2015.04.008>
- 968 Zellweger, F., Coomes, D., Lenoir, J., Depauw, L., Maes, S. L., Wulf, M., Kirby, K. J., Brunet,
969 J., Kopecký, M., Máliš, F., Schmidt, W., Heinrichs, S., den Ouden, J., Jaroszewicz,
970 B., Buyse, G., Spicher, F., Verheyen, K., & De Frenne, P. (2019). Seasonal drivers of
971 understorey temperature buffering in temperate deciduous forests across Europe.
972 *Global Ecology and Biogeography*, 28(12), 1774-1786.
973 <https://doi.org/10.1111/geb.12991>
- 974 Zellweger, F., De Frenne, P., Lenoir, J., Rocchini, D., & Coomes, D. (2019). Advances in
975 Microclimate Ecology Arising from Remote Sensing. *Trends in Ecology & Evolution*,
976 34(4), 327-341. <https://doi.org/10.1016/j.tree.2018.12.012>
- 977 Zellweger, F., De Frenne, P., Lenoir, J., Vangansbeke, P., Verheyen, K., Bernhardt-
978 Römermann, M., Baeten, L., Hédli, R., Berki, I., Brunet, J., Van Calster, H.,
979 Chudomelová, M., Decocq, G., Dirnböck, T., Durak, T., Heinken, T., Jaroszewicz, B.,
980 Kopecký, M., Máliš, F., ... Coomes, D. (2020). Forest microclimate dynamics drive
981 plant responses to warming. *Science*, 368(6492), 772-775.
982 <https://doi.org/10.1126/science.aba6880>
- 983 Zuur, A. F., & Ieno, E. N. (2016). A protocol for conducting and presenting results of
984 regression-type analyses. *Methods in Ecology and Evolution*, 7(6), 636-645.
985 <https://doi.org/10.1111/2041-210X.12577>
- 986
- 987

988

989 8. Supplementary materials

990 8.1. Figures

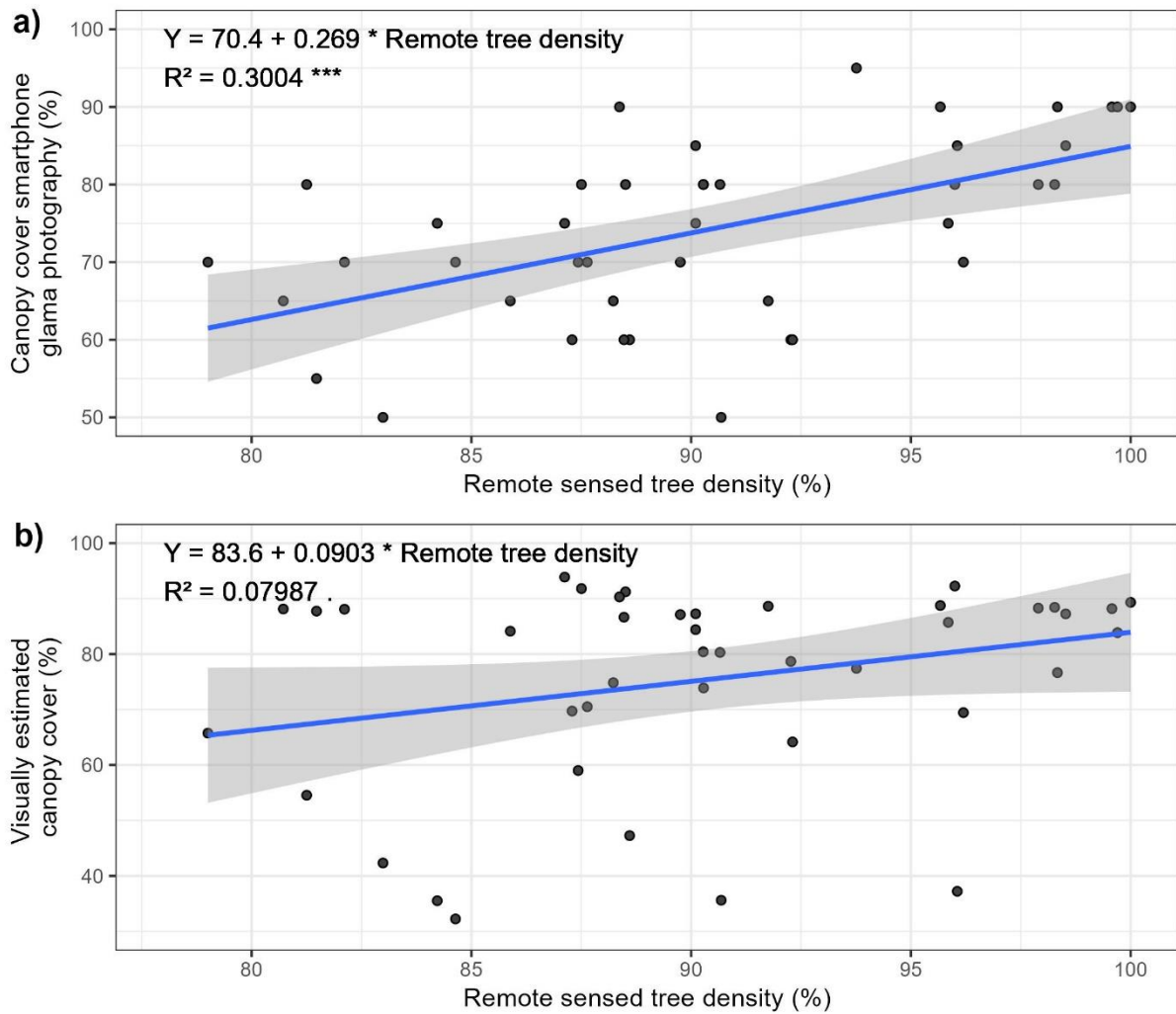


991

992 *Figure S1; Principal component analysis of the spatial factor ought to influence*
993 *microclimate. Axis 1 is explained by elevation and topographic position, Axis 2 represents*
994 *mostly head load index, Axis 3 represents mostly canopy cover. The position in the PCA*
995 *projection of the initial sampling and the final selection of loggers is shown (Lembrechts et*
996 *al., 2021).*

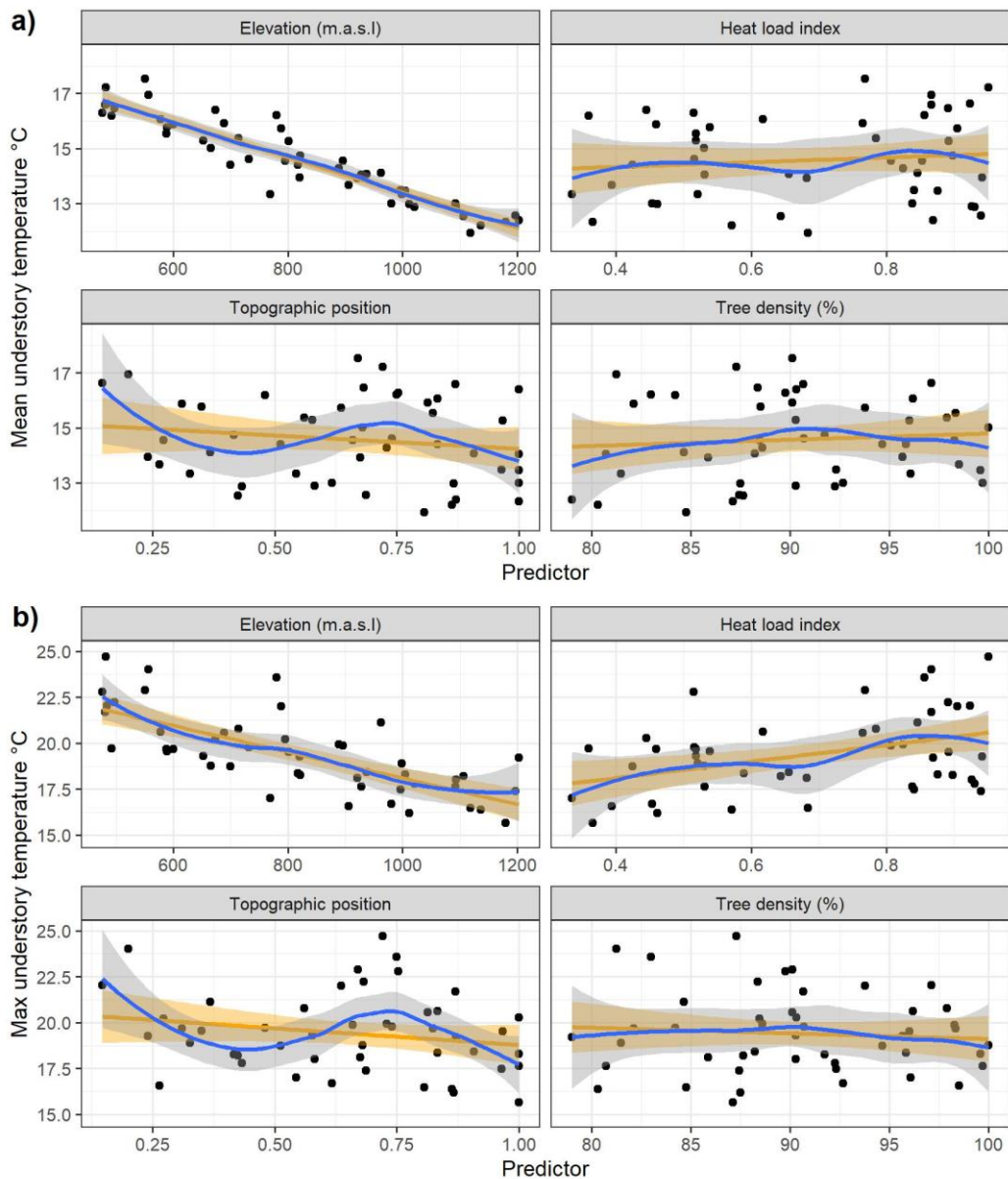
997

998



999

1000 *Figure S2: Relationship between Copernicus remote sensed tree density and canopy closure*
 1001 *estimated in a 25-meter radius circle (a) and canopy cover estimated by a smartphone*
 1002 *photography and segmented by the ‘Glama’ application (b). The blue line corresponds to a*
 1003 *fitted linear model which equation, Person R^2 , and its statistical significance are displayed*
 1004 *(***): $P < 0.001$, (.) $P < 0.1$. The ribbons are the confidence interval of the model.*

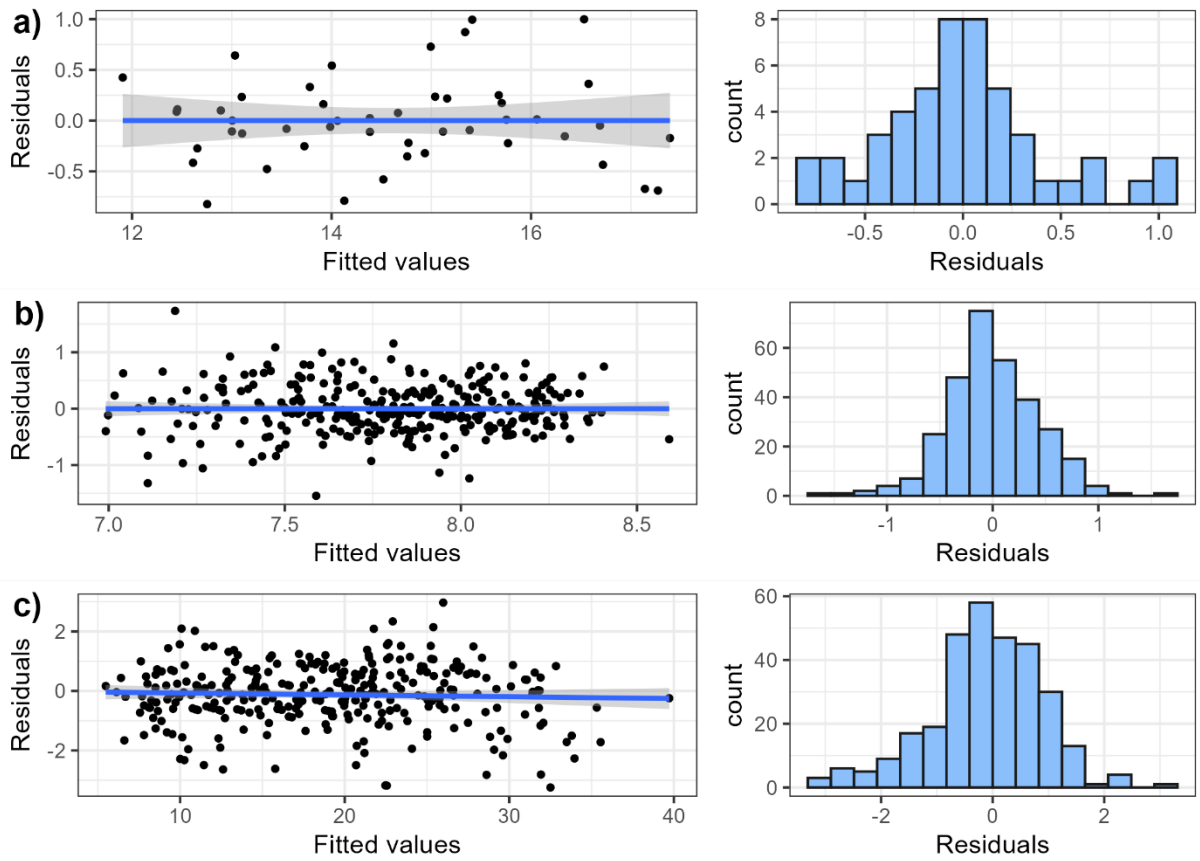


1005

1006 *Figure S3: Relationship between mean and maximum understory temperature of the*
 1007 *growing season with the 4 predictors of the linear temperature model. A loess smoother*
 1008 *(blue) and an univariate linear model (orange) and their confidence interval are also*
 1009 *displayed.*

1010

1011

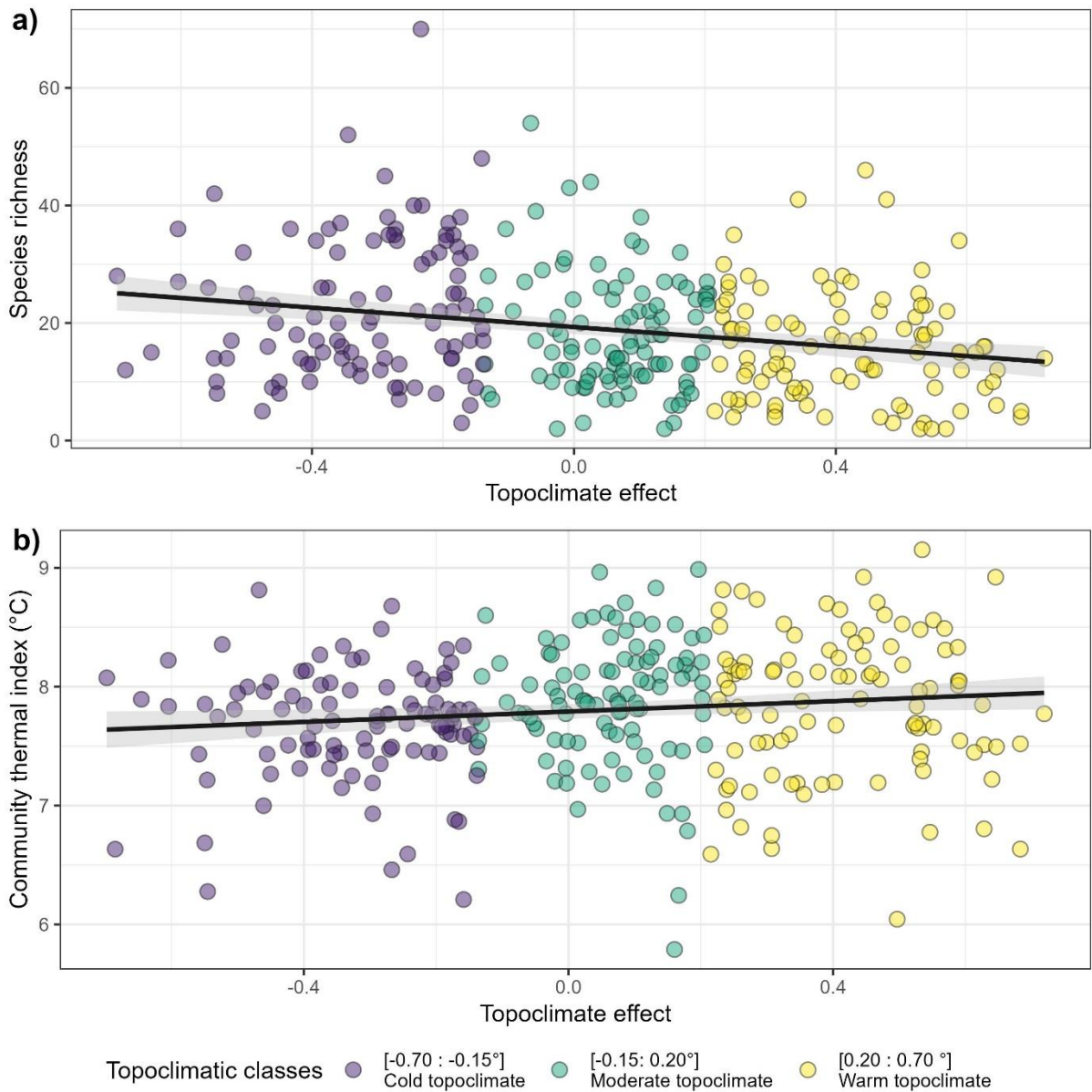


1012

1013 *Figure S4: Relationship between residuals and fitted values, and histogram of residuals of*
 1014 *the linear mean temperature model (a), the CTI linear model (b) and the species richness*
 1015 *negative model (c).*

1016

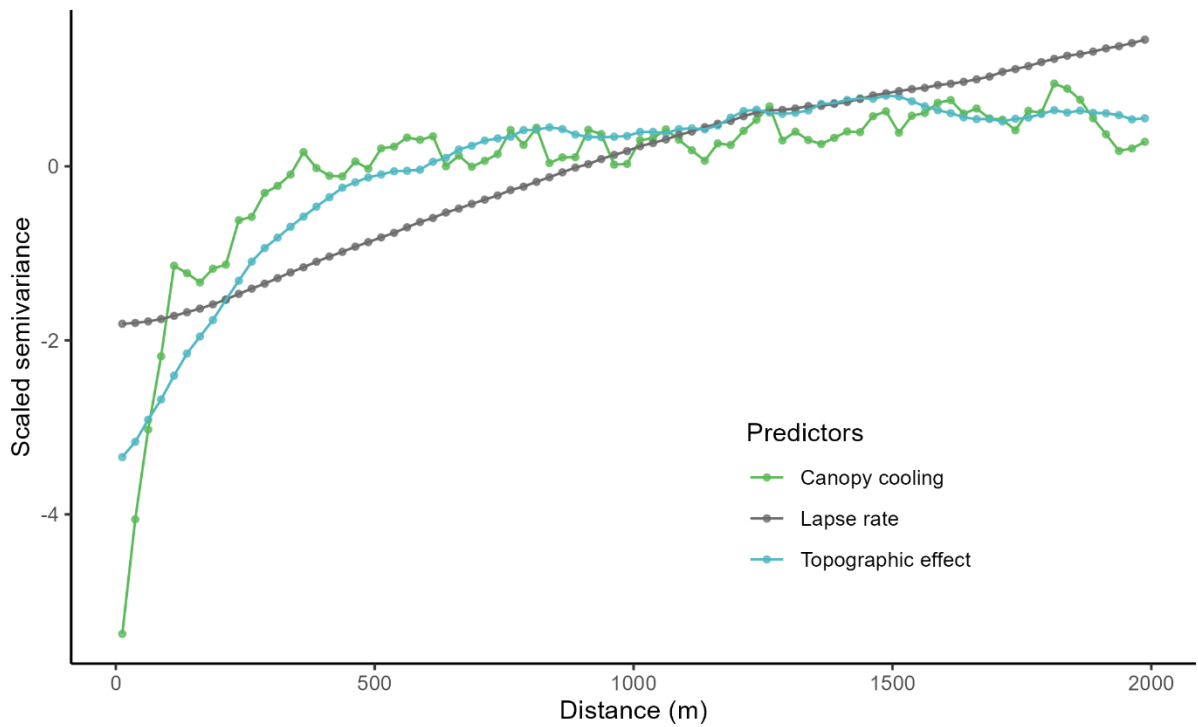
1017



1018

1019 *Figure S5 Species richness (a) and community thermal index (b) of 306 floristic surveys*
 1020 *evenly spread into three topoclimatic buffering classes, as function of predicted*
 1021 *topoclimatic effect on temperature (°C, compared to a moderate topographic situation).*

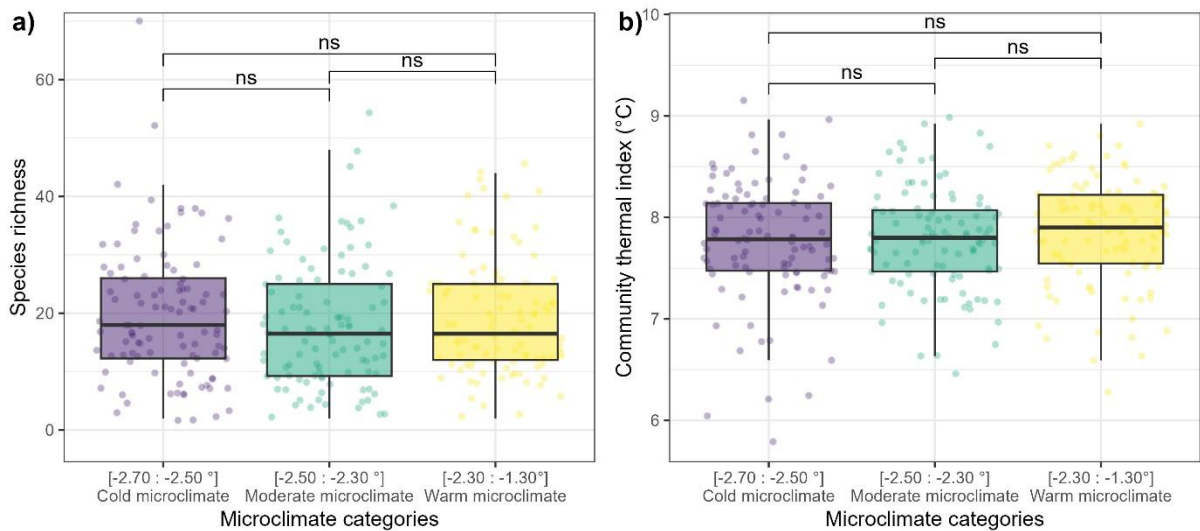
1022



1023

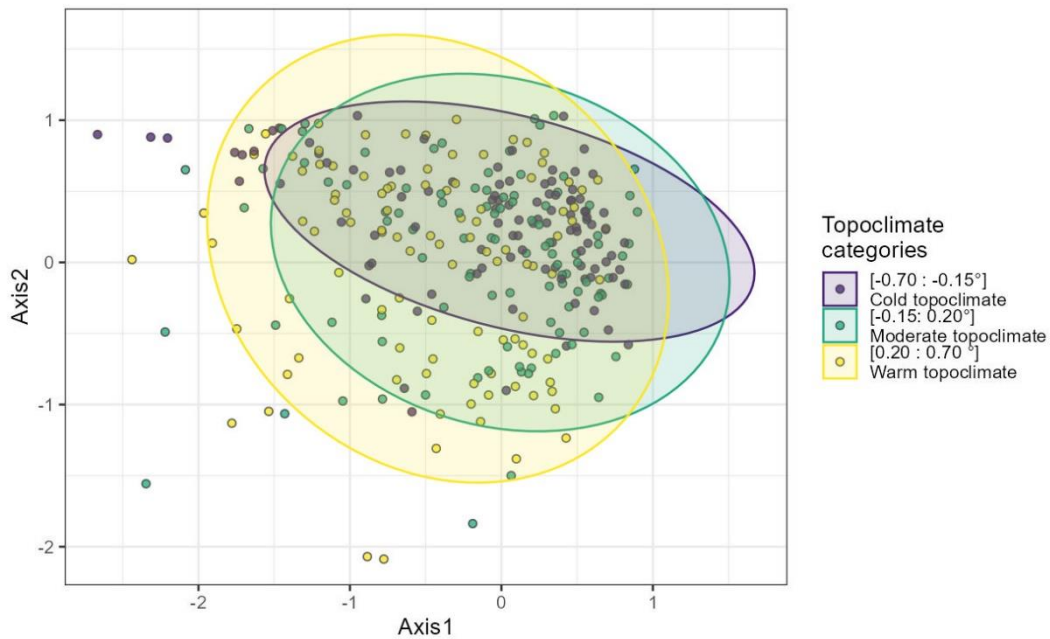
1024 *Figure S6: Variogram of the 3 maps of flora predictors (Figure 2), with a lag of 25m.*
 1025 *Canopy cooling scale semivariance saturates first, followed by topographic effect and the*
 1026 *lapse rate. The saturation of the lapse rate is not shown but is estimated at 6000 m.*

1027



1028

1029 *Figure S7: Species richness (a) and community thermal index (b) of 306 floristic surveys*
 1030 *evenly spread into three microclimatic cooling classes. The p-value significance of a*
 1031 *Wilcoxon test between two classes is displayed as follows: (ns): $p > 0.05$.*



1032

1033 *Figure S8: The first two axes of a correspondence analysis of the 306 floristic surveys spread*
 1034 *among the three topoclimatic cooling class.*

1035

1036

1037

1038

1039

1040 **8.2. Tables**

1041 *Table S1: Summary of the sampling scheme. The left number represents the theoretical*
 1042 *number of plots for the combination of targeted topographic feature and canopy closure*
 1043 *(there were in total 8 strata), the right number represents the number of plots that had*
 1044 *usable temperature data (logger found functioning). All other topographic feature aside*
 1045 *from the targeted one were set to an intermediate value (nor high or low), read M&M 2.3*
 1046 *for more information on the sampling scheme.*

		Canopy closure	
		Low (< 80%)	High (> 80%)
Heat Load Index	Low (< 0.6)	8 - 5	8 - 8
	High (> 0.7)	8 - 5	8 - 8
Topographic Position Index	Low (< 0.2)		8 - 7
	High (> 0.8)		8 - 6
Slope	Low (< 10°)		8 - 4
	High (> 25°)		8 - 5

1047

1048

1049

1050 *Table S2: Estimated parameters, their standard error and p-values of the predictors*
 1051 *included in models of the field canopy closure daily mean growing season temperature. The*
 1052 *range of the predictors in the calibration dataset and their standardized effect size on the*
 1053 *temperature (standard deviation * estimate) are displayed. The percentage of explained*
 1054 *variation per type of predictor is included. P-values were obtained with a Wald test on*
 1055 *parameters.*

Predictor	Type of predictor	Estimate	Standard error	Range	Effect size (°C)	P-value
Intercept (°C)		19.2	0.605			<10 ⁻⁴
Elevation (m a.s.l.)	Elevation	-0.00656	0.000333	475 : 1203	-1.49	<10 ⁻⁴
Heat load index (n.u)	Topography	1.52	0.359	0.335 : 0.951	0.29	<10 ⁻⁴
Topographic index (n.u)	Topography	0.42	0.295	0.201 : 1	0.15	0.163
Canopy closure 25 radius (%)	Canopy	-0.00767	0.00599	50 : 95	-0.092	0.208

1056
1057

1058 *Table S3: Estimated parameters, their standard error and p-values of the predictors*
 1059 *included in models of the immediate canopy closure (i.e. 'Glama' application) daily mean*
 1060 *growing season temperature. The range of the predictors in the calibration dataset and*
 1061 *their standardized effect size on the temperature (standard deviation * estimate) are*
 1062 *displayed. The percentage of explained variation per type of predictor is included. P-values*
 1063 *were obtained with a Wald test on parameters. The canopy cover was estimated visually in*
 1064 *a 25-meter radius circle around the loggers. Immediate canopy cover was measured used a*
 1065 *hemispherical photography above the logger and a sky segmentation application.*

Predictor	Type of predictor	Estimate	Standard error	Range	Effect size (°C)	P-value
Intercept (°C)		16.2	0.812			<10 ⁻⁴
Elevation (m a.s.l.)	Elevation	-0.00672	0.000299	475 : 1203	-1.52	<10 ⁻⁴
Heat load index (n.u)	Topography	5.47	1.22	0.335 : 0.951		<10 ⁻⁴
Topographic index (n.u)	Topography	0.481	0.256	0.147 : 1	0.15	0.0682
Immediate canopy closure (%)	Canopy	0.0346	0.0109	32.23 : 93.88		0.00311
Topography index X Immediate canopy closure	Interaction	-0.0547	0.0162			0.00171

1066 Table S4: Estimated parameters, their standard error and p-values of the predictors
 1067 included in models of the daily maximum growing season temperature. The range of the
 1068 predictors in the calibration dataset and their standardized effect size on the temperature
 1069 (standard deviation * estimate) are displayed. The percentage of explained variation per
 1070 type of predictor is included. P-values were obtained with a Wald test on parameters. Heat
 1071 load and topographic indices have no units, refer to the methods for their calculation.

Predictor	Type of predictor	Estimate	Standard error	Range	Effect size (°C)	Explained variation (%)	P-value
Intercept (°C)		30.6	2.45				<10-4
Elevation (m a.s.l.)	Elevation	-0.00803	0.000685	475.69 : 1203.17	-1.77	56.5	<10-4
Heat load index (n.u)	Topography	5.35	0.732	0.335 : 0.951	1.05	21.5	<10-4
Topographic index (n.u)		0.333	0.607	0.147 : 1	0.081		
Canopy closure (%)	Canopy	-0.0947	0.0253	79.004 : 100	-0.54	3.17	<10-4

1072

1073 Table S5: Estimated parameters, their standard error and p-values of the max temperature
 1074 predictors of the community thermal index (CTI) linear model, and the species richness
 1075 negative binomial generalized linear model. The range of the predictors and their
 1076 standardized effect size on the community predicted variable (standard deviation *
 1077 estimate) are displayed. The P-value is obtained by a Wald test on the parameter. (R² of
 1078 the CTI model: 34.0%)

Model	Predictor	Estimate	Standard error	Range	Effect size	P-value
Species richness	Intercept (°C)	0.307	0.478	NA	NA	0.522
	Lapse rate (°C)	0.0351	0.0156	20.6 : 27.5	1.15	0.024
	Topography effect (°C)	-0.112	0.0271	1.79 : 5.36	-1.76	<10-4
	Canopy cooling (°C)	0.00365	0.035	-9.47 : -4.58	0.0464	0.917
	Bioindicated pH	0.413	0.032	3 : 7.15	7.97	<10-4
Community Thermal Index (°C)	Intercept (°C)	4.57	0.484	NA	NA	<10-4
	Lapse rate (°C)	0.0589	0.0156	20.6 : 27.5	0.106	<10-4
	Topography effect (°C)	0.0965	0.0273	1.79 : 5.36	0.0912	<10-4
	Canopy cooling (°C)	-0.00128	0.0356	-9.47 : -4.58	-0.00093	0.971
	Bioindicated pH	0.268	0.0313	3 : 7.15	0.243	<10-4

1079